

Dynamic Stability and Control: Methods and Developments

by

Melissa Heiser McDaniel

A dissertation submitted to the Graduate Faculty of
Auburn University
in partial fulfillment of the
requirements for the Degree of
Doctor of Philosophy

Auburn Alabama
December 10, 2016

Approved by

Roy Hartfield, Chair, Professor of Aerospace Engineering
John Burkhalter, Professor Emeritus of Aerospace Engineering
Brian Thurow, Professor of Aerospace Engineering
University Reader: Mark Carpenter, Professor of Mathematics and Statistics

Abstract

The purpose of this work is to assess the overall usage, evaluation, and understanding of damping derivatives with a focus on accuracy needs and computational efficiency. With the increased usage of neutrally stable and/or complex airframes, there is increasing desire within the aerospace community to improve the accuracy and understanding of such terms in order to assess the overall flight performance of a vehicle. The current state of the art for damping derivative computations includes the use of semi-empirical methods based on limited simple configuration experimental data or the use of time intensive computational fluid dynamic (CFD) studies. This work proposes that the methodologies used for the calculation of damping derivatives focus on the sensitivity of the system in question to the overall accuracy of the terms. In particular for preliminary configuration work, more accurate but less computationally intensive approaches are desired. A study of the equations of motion has been used to assess the general impacts of damping derivative accuracies for flight vehicles. With the accuracy requirements and sensitivities in mind, new methods and usages have been proposed and developed for the expeditious calculation of these terms in the supersonic flight regime. Theoretical and semi-empirical approaches are presented under the assumption that pitch and roll rates are quite small, resulting in quasi-steady aerodynamic analysis. The use of a component synthesis approach to computing full configuration damping derivatives has been developed as a viable, accurate and expedient approach. Slender body theory damping derivative methodologies have been extended into the supersonic regime to calculate the pitch damping derivatives with improved accuracy. In addition, Evvard's theory has been developed as a compelling approach for determining lifting surface damping derivatives in supersonic flight with sufficient fidelity, flexibility, and expediency for use in conceptual, preliminary and in some cases final design applications for missile systems. Traditional prediction methodologies, such as semi-empirical codes, CFD, and experimental methods

are discussed as comparisons to the new approaches developed in this work. Focus is given to supersonic, low angle of attack configurations with explanations and limitations to the various approaches. The result of this work is a novel, efficient preliminary design approach for accurately estimating damping derivatives on a variety of configurations. The work increases the methods available to aerospace community for the calculation of damping derivatives while illustrating the appropriateness of the various tools for the accuracy required.

Table of Contents

Abstract	ii
List of Figures	v
List of Tables	vii
List of Symbols and Abbreviations.....	ii
1 Introduction.....	1
2 Dynamic Stability and Control	6
2.1 Roll Damping	7
2.2 Pitch Damping Due to Changes in Pitch Rate	8
2.3 Pitch Damping Due to Changes in Angle of Attack Rate	9
3 Current Approaches	11
3.1 Theoretical and Semi-Empirical Approaches	11
3.2 Experimental and Computational Approaches	17
4 Sensitivity Analysis	21
4.1 Acceleration Analysis	23
4.2 Stability Mode Analysis	31
5 Development of Prediction Methods	41
5.1 Modified Slender Body Theory	41
5.2 Evvard's Theory	50

5.3 Angle of Attack Effects	61
6 Verification and Discussion.....	64
4.1 Body Alone Verification	64
4.2 Complete Configuration Verification	70
7 Conclusions and Recommendations	74
References.....	77

List of Figures

Figure 1. Axis System and Notation	7
Figure 2. Change in Local Angle of Attack Due to Roll Rate	8
Figure 3. Illustration of C_{mq} in Flight ²	9
Figure 4. Illustration of $Cm\alpha$ in Flight ²	10
Figure 5. Coordinate System for Apparent Mass Method ²⁶	13
Figure 6. Eastman's Empirical Derivation ³⁰	16
Figure 7. Engineering Accuracy Thoughts ¹⁵	21
Figure 8. Basic Finner Configuration	24
Figure 9. Roll Deceleration Variation with C_{LP}	26
Figure 10. Roll Deceleration Variation with I_{xx}	27
Figure 11. \dot{q} Variations with C_{Mq}	29
Figure 12. \dot{q} Variations with $Cm\alpha$	30
Figure 13. \dot{q} Variations with Inertia	31
Figure 14. Basic Finner Rolling Mode Time Constant Variation with C_l	36
Figure 15. Undamped Natural Frequency Variation with C_{mq}	37
Figure 16. Damping Ratio Variation with C_{mq}	38
Figure 17. Undamped Natural Frequency Variation with $Cm\alpha$	39

Figure 18. Damping Ratio Variation with C_{ma}	39
Figure 20. 9 Caliber Centerbody Curve Fits	44
Figure 21. KE Values Determined from a 7 Caliber Body.....	46
Figure 22. ANSR Configurations ⁴⁶	48
Figure 23. KE as a Function of Xcg Location	48
Figure 24. KE Variation with Body Length.....	50
Figure 25. Mach Line Divisions	51
Figure 26. Schematic of Region of Influence for an Arbitrary Control Point ⁵³	53
Figure 27. Fin Extension into the Body	59
Figure 28. Mach Line Orientations	60
Figure 29. Control Point Determination	61
Figure 30. Updated Rolling Damping Calculations by Moore ⁶⁰	62
Figure 31. Updated Pitch Damping Calculations by Moore ⁶¹	63
Figure 32. 5 Caliber ANSR Results, Mach 1.8.....	65
Figure 33. 5 Caliber ANSR Results, Mach 2.5.....	65
Figure 34. 7 Caliber ANSR Results, XCG=3.25 Calibers Aft of Nose	67
Figure 35. 7 Caliber ANSR Results, XCG=4.036 Calibers aft of Nose	67
Figure 36. 7 Caliber ANSR Results, XCG=4.818 Calibers Aft of Nose	68
Figure 37. 9 Caliber ANSRResults, Mach 1.8.....	69
Figure 38. 9 Caliber ANSR Results, Mach 2.5.....	69
Figure 39. Results for Basic Finner Roll Damping.....	71
Figure 40. Modified Finner Geometry.....	72
Figure 41. Modified Finner Clp	73

List of Tables

Table 1. Missile Datcom Predicted Values of Cl _p	25
Table 2. Missile Datcom Longitudinal Predictions	28
Table 3. Lateral Aerodynamics of the Basic Finner	35
Table 4. Basic Finner Longitudinal Aerodynamics	36
Table 5. Differential Pressure Equations Due to Rolling Motion, Supersonic Leading Edge ⁵³	54
Table 6. Differential Pressure Equations Due to Rolling Motion, Subsonic Leading Edge ⁵³	55
Table 7. Pressure Coefficient Due to a Pitching Rate ⁵⁷	57
Table 8. Pressure Coefficient Due to a Rate of Change in Angle of Attack ⁵⁸	58

List of Symbols and Abbreviations

Roman Letters

b	Wing span
b/2	Exposed wing semi-span
cal	Calibers
cent	Centroid
CG	Center of gravity
C_{ll}	Rolling moment coefficient
C_{lp}	Roll damping moment coefficient
C_M	Pitching moment coefficient
$C_{M\alpha}$	Pitching moment derivative with respect to angle of attack
$C_{m\dot{\alpha}}$	Pitch damping moment coefficient due to angle of attack rate
C_{Mq}	Pitch damping moment coefficient due to pitch rate
CN	Normal force coefficient
$C_{N\alpha}$	Normal force derivative with respect to angle of attack
C_{Mq}	Pitch damping moment coefficient due to pitch rate
$C_{M\alpha}$	Pitching moment derivative with respect to angle of attack
C_R	Root chord length
C_T	Tip chord length

I_{xx}, I_{yy}	Moments of Inertia
M	Mach number
Q	Dynamic pressure
q	Pitch rate (radians/sec)
p	Roll rate (radians/sec)
S_{ref}, S_{base}, S	Reference Areas
U	Freestream Velocity
u, v, w	Velocity components in the x, y, and z directions
x, y, z	Coordinate system axis x-streamwise, y-spanwise, z-chordwise

Greek Letters

α	Angle of attack
$\dot{\alpha}$	Rate of change of angle of attack (radians/sec)
B	$\sqrt{M^2 - 1}$
ρ	Density of air
δ	Angle of panel normal with z-axis
Φ	Velocity potential function
λ	Eigenvalue of the stability matrix
Λ_{LE}	Sweep angle at leading edge
Λ_{TE}	Sweep angle at trailing edge
μ	Mach angle

1 Introduction

During the first six decades of the 20th century, the calculation of aerodynamic loads was nearly entirely an analytic endeavor with effective methods developed for the estimation of loads for air vehicle design applications. In about 1960, the digital computer began to gradually permeate the aerospace design activity and numerical methods increased in usage and entirely numeric techniques such as direct numerical solutions to flow equations were developed and matured to an advanced state. A range of methods have been developed to determine the aerodynamic characteristics of a variety of body shapes, fin designs, and body and fin configurations. These efforts have resulted in development of numerous codes for rapid and accurate prediction of configuration aerodynamics. However, the majority of this effort has focused on the static aerodynamics of a configuration, i.e. the forces and moments acting on a vehicle at a fixed orientation in steady flow. This analysis has become the basis of most theoretical, empirical, experimental and computational approaches to aerodynamics. However, this type of analysis does not fully encompass the flight behavior of a moving vehicle.

In free flight, a vehicle is subjected to six degrees of freedom. These are translation and rotation about the x, y, and z axes. Although the aerodynamics may be considered static over all portions of the flight, the ability to maneuver indicates that dynamic behavior must also be analyzed. Specifically for flight simulations, the dynamic behavior of a system must be considered. Flight simulations are increasingly used to assess the performance of a flight vehicle as a whole and allowing for issues to be resolved before costly flight testing. As flight vehicles and control systems become more complex, non-linear models are required for simulations. This necessitates an understanding of the vehicles response to various disturbances (missile simulation). To fully understand the aerodynamics of a flight vehicle such as a missile or airplane, the dynamic properties of the vehicle must also be understood. Such understanding requires knowledge of the vehicles' response to rotational

motion; also known as the damping of the system. In other words, once disturbed from its initial flight path, does the vehicle return to steady state flight? If so, how quickly does that occur?

In basic terms, static stability is the predisposition of a system to return to or deviate from its equilibrium position after a disturbance. How the system returns to (or deviates from) that point is not considered. Dynamic stability, on the other hand, is concerned with the entire history of the motion, in particular the rate at which the motion damps out¹. Static stability is a requirement for dynamic stability, i.e. a statically unstable airframe cannot be dynamically stable. However, a statically stable aircraft may be dynamically unstable. In other words, certain motions may be amplified rather than damped². Knowledge of dynamic stability is required in the pitch, roll, and yaw planes; however, motions in two of the planes can uncoupled from each other. Pitching motions do not typically induce rolling or yawing motions while rolling and yawing motions do not induce pitching motions. While this is technically possible given certain mass, inertia, and aerodynamic characteristics, this assumption allows methods to be developed and tested independently. Additionally, it allows the aerodynamicist to easily determine which terms are of most importance to a given configuration.

Damping derivatives or dynamic stability have often been considered a second order effect. As a result, there was little reason to accurately calculate these terms in most missile simulations. However, with the increase in highly maneuverable airframes and low inertia systems, dynamic stability calculations is rapidly becoming an area of interest within the aerospace community. One of the inherent issues with the prediction of damping derivatives results from the fact that it is an unsteady effect. The majority of aerodynamic prediction codes available to the engineer either do not have the capability to model unsteady aerodynamics while computational methods are time intensive in their calculations. However, research has shown that some steady state theoretical methods may be expanded to include the calculation of damping derivatives, most notably classic slender body theory³. A notable feature of damping derivative calculations is that a build-up approach can be used for their calculation. That is, the body and lifting surfaces can be calculated separately with appropriate theories and the results synthesized as they are for

static aerodynamics^{4,5}. Although this approach is well verified for static calculations, it has not been exploited for dynamic computations.

Another consideration in the computation of dynamic stability is an understanding of the required accuracy and effects of the dynamic stability on a flight vehicle. These effects are completely dependent on the system under consideration. With regard to these effects, the desired accuracy may be dependent on the computational or experimental background of the engineer and could require a shift in the aerospace community understanding of these problems. In particular, it is important to trade the computational cost of such calculations with the required accuracy, particularly in the preliminary design phase.

There are several methods currently available to the aerodynamicist for the calculation of damping derivatives, each with their own advantages and disadvantages. The primary method is a semi-empirical aerodynamic prediction tool, such as Missile Datcom, MISL3, or AP09⁶⁻⁸. These codes have exceptionally short run times, allowing the engineer to analyze multiple configurations rapidly. However, the damping methodologies in these codes are based on very limited sets of empirical data and therefore have restricted applicability to complex configurations.

Another option is the use of ground based testing. This includes both free flight testing and wind tunnel testing. For free flight testing, a spark range can be utilized. In this set up, a test article is fired in an indoor range and multiple, high speed images are obtained during flight. From these images, the aerodynamics of the vehicle can be determined. This is the most common method utilized for projectiles in the United States^{9,10}. While useful, there is often a significant amount of scatter in the results, leading to high uncertainty. Wind tunnel testing may have more accuracy as the uncertainties are better known and less open to interpretation; however, the test mechanisms are complex and expensive, particularly when pitch damping results are desired. For roll damping tests, a free roll sting may be utilized¹¹. In this type of testing, the model is spun to a predetermined rate and allowed to decay over the course of the run. From the decay, the roll damping may be determined. Pitch damping requires a more complex setup of cables or sting testing¹¹⁻¹⁴. In this type of sting testing, the model is typically forced to oscillate

at a given rate and the damping is then calculated. Due to the complexity of the test configurations and models, these methods are seldom used.

With the advent of faster computers over the last several decades, numerical computations have been more popular for the computation of rate damping derivatives. These computations include both inviscid and full viscous Navier-Stokes solutions¹⁵⁻²². Oftentimes, these methods require complex, time-accurate solutions though some work has been done using steady-state methods^{18,21,22}. The results match well with available test data; however, considerable expertise is required in the development of the solution and even with today's high speed processing, results can be time consuming. Oftentimes, the level of precision obtained by these means is not needed by the engineer in the preliminary design phase.

With the existing methods and requirements in mind, the work provides an assessment of the usage, evaluation and understanding of damping derivatives with a focus on accuracy requirements and computational efficiency. A study of the equations of motion has been used to assess the general impacts of damping derivative accuracies for flight vehicles. In addition, new and novel methods and approaches have been proposed and developed for the expeditious calculation of these terms for supersonic configurations. Theoretical and semi-empirical approaches are developed under the assumption that pitch and roll rates are quite small, resulting in quasi-steady aerodynamic analysis. In particular, slender body theory has been expanded to the supersonic regime while Evvard's theory has been developed as a compelling approach for determining damping derivatives. A body build up approach is applied to these methods in order to expedite results while improving the accuracy of traditional semi-empirical approaches. Comparisons between prediction methods and experimental data are presented to assess the various approaches developed. The present work develops a methodology to provide the engineer with a means to rapidly and accurately predict the pitch and roll damping of arbitrary configurations comprised of a body and lifting surfaces. The methods formulated in this work are based in potential flow theory and the theories are tailored to the component being analyzed, thereby exploiting the body build-up approach. Semi-empirical methods are also employed to improve results where applicable. With this type of approach come some inherent

assumptions. The primary assumption is that the flow must remain attached, which is a necessary requirement for potential flow. Additionally, pitch and roll rates are relatively small so as to represent a quasi-steady state condition rather than a complete unsteady analysis of the flow field²³. Traditional prediction methodologies, such as semi-empirical codes, CFD, and experimental methods are discussed as comparisons to the new approaches developed in this work. Focus is given to supersonic, low angle of attack configurations with explanations and limitations to the various approaches. The result of this work is a novel, efficient preliminary design approach for accurately estimating damping derivatives on a variety of configurations. The work increases the methods available to aerospace community for the calculation of damping derivatives while illustrating the appropriateness of the various tools for the accuracy required.

2 Dynamic Stability and Control

Derivatives are often used to assess the stability properties of a vehicle. Typically, there are three common stability derivatives that are considered by the aerodynamicist. The first is static stability derivatives. These derivatives quantify the change in force and moment due to a change in a flight parameter, such as angle of attack. Terms such as $C_{m\alpha}$ fall into the category of static stability derivatives. The second type of derivatives are the control derivatives, such as $C_{m\delta}$. These derivatives quantify the change in forces and moments due to small changes in control fin deflection. The final set of derivatives are the focus of this effort and are the dynamic stability derivatives. They are also referred to as the damping derivatives. While important to the overall flight dynamics of a vehicle, these terms are often poorly understood and calculated by the engineer.

In practical terms, the “damping derivatives” are those forces and moments that oppose the motion of a vehicle. As a missile rapidly maneuvers in flight, additional velocities are induced on the vehicle thereby inducing an angle of attack^{2,5}. The moment opposing this induced velocity is known as the damping moment. In general, the pitch damping and the roll damping terms are of most interest to the engineer. The pitch damping is comprised of both a change in pitch rate and a change in angle of attack. The rotations are centered about a spanwise axis through the center of gravity of the vehicle. Thus, moving the center of gravity will affect the computation of the pitch damping terms. The roll damping is brought about by a rotation about the vehicles’ longitudinal axis. Figure 1 shows a standard axis system as well as the pitch rate (q), change in angle of attack (α) and roll rate (p). This section discusses the basic physics that result in the presence of the damping derivatives.

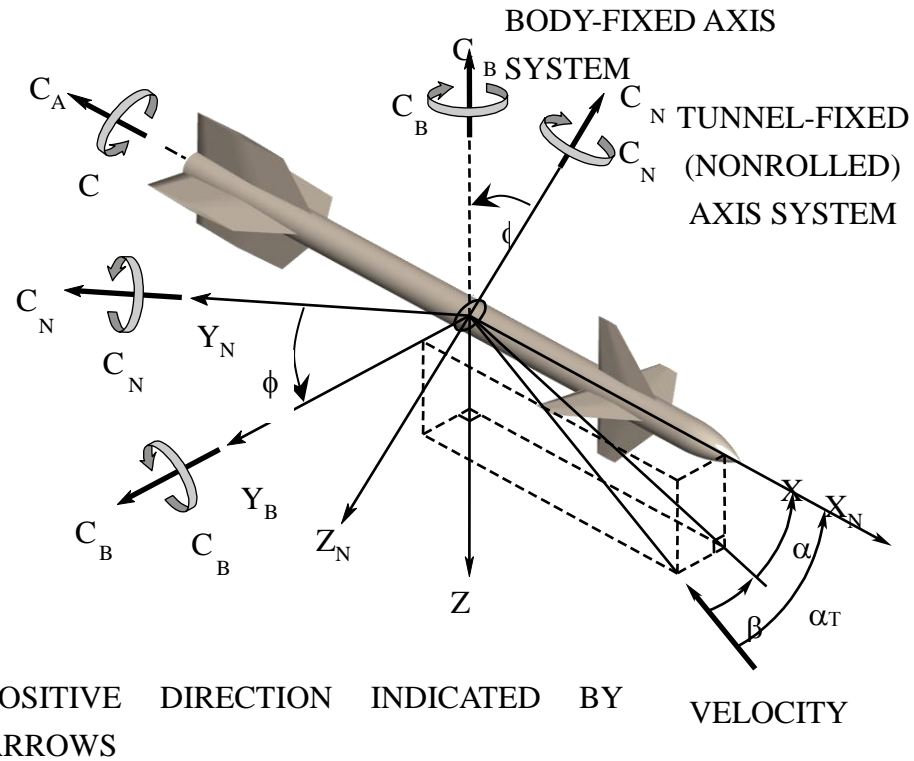


Figure 1. Axis System and Notation

2.1 Roll Damping

A rolling motion is defined as a rotation about a vehicles' longitudinal, or x-axis as shown in Figure 1. The resistance of a vehicle to this rolling motion is known as the roll damping, C_{lp} . Unless very large roll rates are considered, the primary contribution to the roll damping is through the lifting surfaces. However, a roll rate will affect all of the lifting surfaces on a vehicle regardless of the rate of rotation. As the vehicle rolls about its longitudinal axis the spanwise angle of attack of the surface is altered, as shown in Figure 2. The angle of attack at any span wise location is related to the roll rate through the relation $\rho y/2V$ where y is distance from the body centerline to the span location of interest.

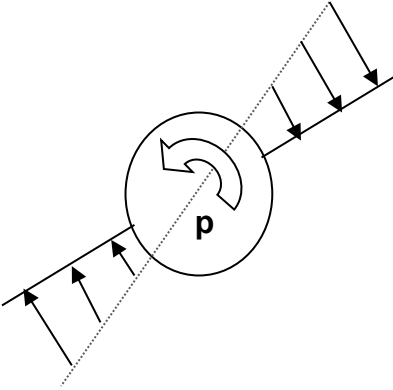


Figure 2. Change in Local Angle of Attack Due to Roll Rate

As a consequence of the angle of attack variation, the lift is varied along the span of the wing. As long as the flow remains attached, this induced lift will always oppose the roll rate, thereby damping the motion^{2,5,24}. With knowledge of the lift force at each span wise location, the roll damping moment can be directly calculated. In practice, this is difficult as the loading is heavily dependent on the aspect ratio, sweep angle, taper ratio, and Mach number of the surface. Methods to calculate the roll damping are the focus of this effort and are derived in later sections. The roll damping may have a significant impact on the handling and controllability of a vehicle. These potential effects are discussed in section 4.

2.2 Pitch Damping Due to Changes in Pitch Rate

The pitch damping derivative is actually the sum of two terms, the change in pitching moment due to a change in pitch rate (C_{mq}) and the change in pitching moment due to a change in the angle of attack rate (C_{ma}). The pitch rate can be thought of as a rotation about a spanwise axis passing through center of gravity while the angle of attack remains nearly constant, similar to Figure 3. A steady pitch up or pull up maneuver is typical of this type of motion. As with the rolling motion, all lifting surfaces are affected through a change in their local angle of attack. However, the body can no longer be neglected, particularly for missile configurations where it may contribute up to 30 percent of the total damping in pitch. Assuming a positive vertical change in pitch rate, lifting surfaces fully behind the

CG will experience an increase in local angle of attack thereby increasing the normal force and ultimately creating a negative (i.e. restoring) pitching moment. Surfaces closer to the CG (such as an airplane wing) can have both an increase and decrease in the local angle of attack depending on the relative location to the CG. These surfaces typically have lower contributions to the pitch damping as the moment arm is smaller, but they should not be neglected.

In the analysis of C_{mq} , it is assumed that the instantaneous forces correspond to instantaneous angles of attack. In other words, any lag due to viscosity is not taken into account^{2,22}. This is done in most analysis to simplify the equations of motion and is an additional requirement if potential flow techniques are desired.



Figure 3. Illustration of C_{mq} in Flight²

2.3 Pitch Damping Due to Changes in Angle of Attack Rate

The change in pitching moment due to a time rate change of angle of attack $C_{m\dot{\alpha}}$ is a more complicated term than the change due to pitch rate. This motion is a change in angle of attack with constant pitch rate, as depicted in Figure 4. Its complexity results from the fact that it is an inherently unsteady flow condition that makes analysis by quasi steady state methods difficult. Unlike the C_{mq} term where it was assumed that changes occurred instantly, the $\dot{\alpha}$ derivatives exist because the pressure distribution over a lifting surface does *not* adjust itself instantaneously when the angle of attack is altered². Therefore the lift has a transient response that is dependent on the Mach number. Fortunately the

characteristic frequencies are usually quite small, making it a lower contribution to the overall pitch damping term.

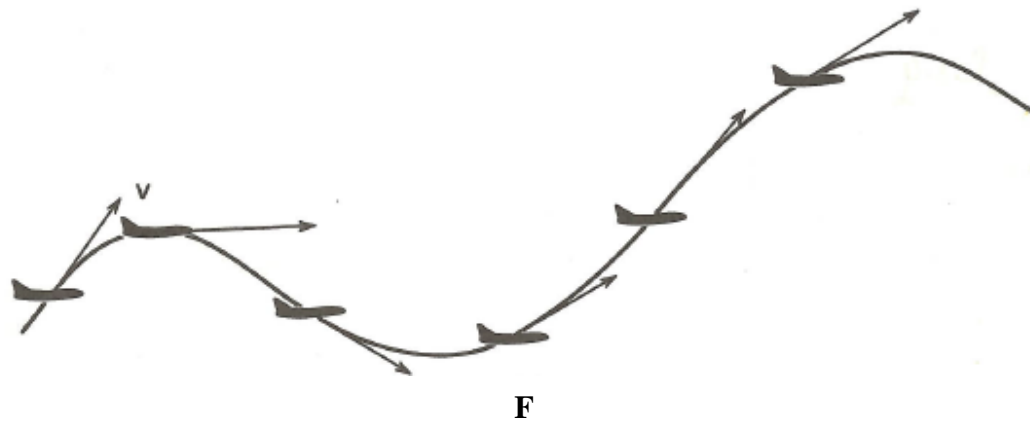


Figure 4. Illustration of $C_{m\dot{\alpha}}$ in Flight²

3 Current Approaches

The previous section was intended define the damping derivative terms that are the focus of this effort. These terms require both an accurate and flexible approach due to the importance of the terms for given flight vehicle designs. Many of the methods currently employed by engineers have several limitations in their application geometries or conditions. However, several may offer ways to expand current damping derivative methodologies to evaluate a wider range of configurations. This section provides a brief presentation of the currently available state of the art methods for damping derivatives. These methods were used as a starting point in the development of new methodologies for damping derivative calculation. Experimental and computational approaches are presented as they will provide the basis for validation of the updated approaches developed for this effort.

3.1 Theoretical and Semi-Empirical Approaches

Most all of the approaches available to the engineer have their basis in potential flow theory. The velocity potential, ϕ , is a scalar representation of position and time in a flow. Differentiation of the potential yields the velocities. The velocity potential can be written for both compressible and incompressible flows as well as in a non-linear or linearized form. For the purpose of this effort, most theories make use of the linearized equations. The following sections present the most common theoretical approaches for calculating the damping derivatives.

3.1.1 Slender Body Theory

Slender Body Theory is a linearized potential flow solution for calculating the aerodynamics of a body of revolution at angle of attack. By restricting the flow to small

perturbations and using both continuity and Newton's equations of motions, the partial differential equation governing flow around a slender body can be written as in equation 1.⁷

$$\beta^2 \varphi_{xx} + \varphi_{yy} + \varphi_{zz} = 0 \quad (1)$$

Furthermore, slender body theory prohibits velocity perturbations in the longitudinal direction which further reduces the governing equation to Laplace's equation.

$$\varphi_{yy} + \varphi_{zz} = 0 \quad (2)$$

This equation defines the flow conditions in any plane that is perpendicular the longitudinal axis. The resulting flow, and therefore the loading, is independent of Mach number, so results are valid across the entire speed regime.

Slender Body theory is commonly used to calculate the static aerodynamic coefficients. The key result of the theory, as stated by Nielsen²⁵, is that that normal force of a slender body is based only on its base area. It also produces a constant value for the normal force slope that is again independent of Mach number.

$$C_N = 2\alpha \frac{S_{base}}{S_{ref}} \quad C_{N\alpha} = 2 \frac{S_{base}}{S_{ref}} \quad (3)$$

In this form, slender body theory only accounts for the effects of body thickness and angle of attack. It is not possible to obtain the effects due to pitching motions that are required to obtain the damping derivatives. However, modifications such as the use of apparent mass terms have made this possible. The remainder of this section discusses how slender body theory can be utilized to calculate damping derivatives and modifications that are available to further improve that theory.

3.1.2 Bryson's Slender Body Theory

Basic slender body theory as defined above does not place any restrictions on the shape of a body, provided that flow perturbations resulting from the presence of the body

are small. As a result, calculations from the theory are best for axisymmetric bodies. However, the addition of the apparent mass method (or apparent area depending on the reference) as developed by Bryson²⁶ extends slender body theory to a wider variety of bodies and permits direct calculation of the stability derivatives. Detailed explanation of this method is presented by Bryson²⁶ and Nielsen²⁵. For this method, the inertial properties of a cross section must be known. Several examples for assessing this are provided by Nielson. A coordinate system for the analysis is provided in Figure 5.

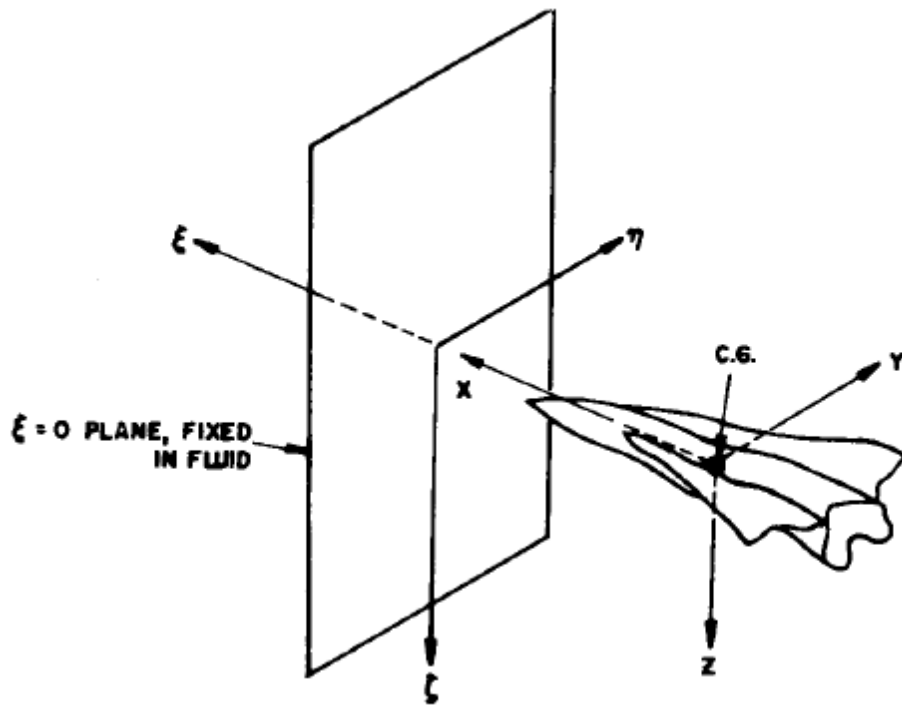


Figure 5. Coordinate System for Apparent Mass Method²⁶

Bryson²⁶ defined the kinetic energy per unit length in the η - ζ plane in equation 4 as

$$T' = \frac{1}{2} \rho S[v, w, pD][A] \begin{bmatrix} v \\ w \\ pD \end{bmatrix} \quad (4)$$

where v , w , and pD are velocities in the x y and z directions and A is a symmetric matrix containing the apparent mass or inertial coefficients. These are defined as in equation 5.

$$\begin{bmatrix} A_{11} & A_{12} & A_{13} \\ A_{21} & A_{22} & A_{23} \\ A_{31} & A_{32} & A_{33} \end{bmatrix} = -\frac{1}{S_{ref}} \begin{bmatrix} \oint \varphi_1 \frac{\partial \varphi_1}{\partial n} dS & \oint \varphi_1 \frac{\partial \varphi_2}{\partial n} dS & \frac{1}{D} \oint \varphi_1 \frac{\partial \varphi_3}{\partial n} dS \\ \oint \varphi_1 \frac{\partial \varphi_2}{\partial n} dS & \oint \varphi_2 \frac{\partial \varphi_2}{\partial n} dS & \frac{1}{D} \oint \varphi_2 \frac{\partial \varphi_3}{\partial n} dS \\ \frac{1}{D} \oint \varphi_1 \frac{\partial \varphi_3}{\partial n} dS & \frac{1}{D} \oint \varphi_2 \frac{\partial \varphi_3}{\partial n} dS & \frac{1}{D} \oint \varphi_3 \frac{\partial \varphi_3}{\partial n} dS \end{bmatrix} \quad (5)$$

These inertia coefficients are specific to a given cross section. Using this kinetic energy, the forces acting on the body can be developed. A rigorous derivation can be found in either Bryson or Nielsen. Of most interest for this analysis are the normal force and pitching moment coefficients. Additionally, only those terms that are functions of α , q and $\dot{\alpha}$ are necessary for the calculation of the pitch damping derivatives. These simplified functions are shown in equations 6 and 7.

$$C_N = -C_z = 2A_{22} \left(\alpha + \frac{qD}{U} \frac{x_b}{D} \right) + 2 \int_0^L A_{22} d\left(\frac{X}{D}\right) \left(\frac{\dot{\alpha}D}{U} \right) \quad (6)$$

$$\begin{aligned} C_m = -2 \frac{x_b}{D} A_{22} \left(\alpha + \frac{qD}{U} \frac{x_b}{D} \right) &+ 2\alpha \int_0^L A_{22} d\left(\frac{X}{D}\right) \\ &+ 2 \left(\frac{\dot{\alpha}D}{U} - \frac{qD}{U} + \alpha \frac{U\dot{D}}{U^2} \right) \int_0^L A_{22} \left(\frac{X}{D} \right) d\left(\frac{X}{D}\right) \\ &- 2 \left(\frac{pD}{U} \frac{qD}{U} \right) \int_0^L A_{12} \left(\frac{X}{D} \right)^2 d\left(\frac{X}{D}\right) \end{aligned} \quad (7)$$

From Nielson²⁵, the apparent mass terms appearing above for a circular body are defined in equations 8 and 9, with r equal to the body radius and S equal to the reference area.

$$A_{22} = \frac{m_{22}}{\rho S} = \frac{\pi \rho r^2}{\rho S} = 1 \quad (8)$$

$$A_{12} = \frac{m_{12}}{\rho S} = 0 \quad (9)$$

Recognizing that $C_{N\alpha} = \frac{\partial C_N}{\partial \alpha}$, the basic slender body value of 2 is obtained. Now, to calculate the damping derivatives, equations 10-12 are utilized.

$$C_{mq} = \frac{\partial C_m}{\partial \left(\frac{qD}{2U}\right)} = -4 \left(\frac{x_B}{D}\right)^2 - \frac{1}{3} \left(\frac{l}{D}\right)^2 \left(\frac{x_B}{D}\right) \quad (10)$$

$$C_{m\dot{\alpha}} = \frac{\partial C_m}{\partial \left(\frac{\dot{\alpha}D}{2U}\right)} = \frac{1}{3} \left(\frac{l}{D}\right)^2 \left(\frac{x_B}{D}\right) \quad (11)$$

$$C_{m\theta} = C_{mq} + C_{m\dot{\alpha}} = -4 \left(\frac{x_B}{D}\right)^2 = -4 \left(\frac{l}{D} - \frac{X_{MRP}}{D}\right)^2 = -2C_{N\alpha} \left(1 - \frac{X_{MRP}}{L}\right)^2 \left(\frac{l}{D}\right)^2 \quad (12)$$

Note that the factor of 2.0 has been added to account for a consistent normalization of q and $\dot{\alpha}$. Bryson normalizes by qD/V while this work normalizes by $qd/2V$.

It is clear from these equations that pitch damping derivatives calculated by this method will not vary with Mach number. In practice, the method will not perform well for most configurations²⁷. However, it is an excellent starting point for modified theories.

3.1.3 $C_{l\delta}$ Approach to Roll Damping

The most common empirical approaches for calculating the roll damping of finned vehicles relate the values of C_{lp} and $C_{l\delta}$. Initial theoretical results from Bolz and Nicolades²⁸ produced by the relation shown in equation 13

$$\frac{C_{lp}}{C_{l\delta}} = -0.627 \frac{d}{b_o} \quad (13)$$

where b_o refers to the total span including the body. Subsequently, Adams and Dugan²⁹ produced a near identical relation, without the diameter to span relation. These approaches were never applied to any experimental data and subsequently were found to be insufficient for most configurations.

Eastman³⁰ found the available theoretical approaches insufficient to match the experimental data available at the time. As a result, he expanded on these theoretical methods to create a fully empirical approach based on the relation of C_{lp} and $C_{l\delta}$. His method requires knowledge of Y area centroid (Y_{cent}) of the fin. This distance is measured radially from the body centerline to the centroid of the exposed fin. This empirical

correlation was determined from wind tunnel data on configurations shown in Figure 6. The graph used for his correlation is also shown in Figure 6.

Symbol	Reference	Geometry	Comments
---	1 THRU 5		Basic Finned, approximate average of much data
□	3,4		Modified Finner C_{L_p} estimated
△	6		Folding fin rocket
◊	7		Low speed only
■	8		Boeing model with 5 different tails Tail shapes: b/c b/d 0.90 0.70 0.70 0.62 0.47 0.62 0.69 0.75 0.48 0.52 ■ = range and average of data for 5 tails

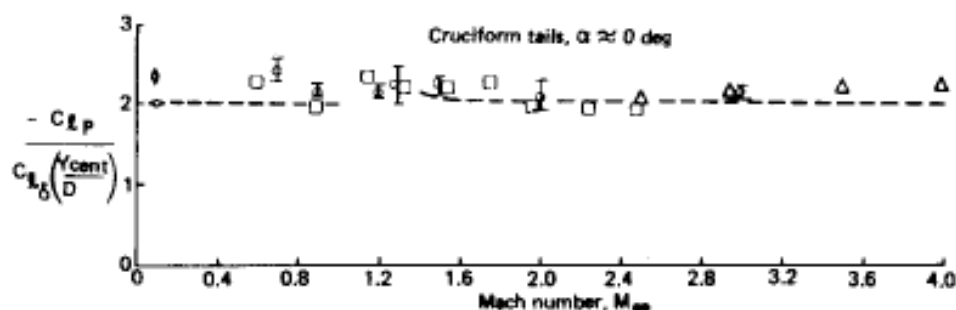


Figure 6. Eastman's Empirical Derivation³⁰

His method presents the roll damping as in equation 14.

$$C_{lp} = -2.15 \frac{Y_{cent}}{D} C_{l\delta} \quad (14)$$

The simplicity of the calculation lends itself for use when wind tunnel data is available and the configuration is simple. There is no need to vary the method for different Mach regimes. However, its simplicity is also its limiting factor. Although the configurations used for correlation are widely varied, the available data appears to be small. Additionally, it is only applicable to configurations with a single fin set, thereby eliminating its use for a wide variety of missile variations.

3.2 Experimental and Computational Approaches

The standard state of the art metric for the assessment of rapid prediction methods is the use of experimental data. Typically this includes wind tunnel test or flight data. There are several methods for wind tunnel testing that will be briefly discussed in this section. The purpose of this section is to provide an overview of the methods. References are provided for a more exact discussion of the procedures used in determine the damping derivatives from these experimental setups.

3.2.1 Wind Tunnel Testing

For most aerodynamicists, wind tunnel testing represents the “gold standard” for obtaining accurate aerodynamic characteristics and data. While most wind tunnel tests are performed to obtain static aerodynamic data, there are a variety of ways to obtain dynamic data in the wind tunnel. However, with cost as a driver this approach is not usually taken unless the dynamic derivatives are considered critical to understanding the overall behavior of the flight vehicle. Most dynamic tests are focused on aero elastic effects rather than damping derivatives due to the relative importance of the terms³¹.

The “easiest” dynamic stability term to obtain in the wind tunnel is the roll damping. The most common method to measure roll damping is through the use of a spin rig. In this

type of setup, the model is mounted to a sting as is typical of most missile wind tunnel set ups; however, the body is allowed to roll freely around the balance. The test article is mechanically spun and a tachometer is used to measure the spin rate variation over the course of a wind tunnel run. With this information, it is possible to determine the roll damping via the following equation.

$$C_{lp} = \frac{2V(I_{xx}\dot{p} - C_{lx}q_\infty S_{ref}d_{ref} - L_{bearing\ friciton})}{pq_\infty S_{ref}d_{ref}^2} \quad (15)$$

In equation 15, I_{xx} represents the x (or roll) axis moment of inertia of the body, \dot{p} is the tachometer measure roll rate, C_{lx} is the static rolling moment of the vehicle, and $L_{bearing_friction}$ is the rolling resistance measured on the bearings for the spin rig.

Pitch damping is more complicated to obtain in the wind tunnel. There are two primary approaches: Free-oscillation testing and forced-oscillation testing.^{13, 14, 31} In free-oscillation testing, the model is mounted on a 1 degree of freedom small amplitude sting. Stable models are perturbed using a forced air approach to disturb the setup while unstable vehicles are allowed to freely move on the sting with increasing amplitude. Oscillations are measured with a tachometer and pitch damping is obtained in a method similar to that described for the roll damping.

In forced oscillation testing, the model is mechanically driven to a specific oscillating frequency. This method is more complex than the free-oscillation setup; however, it allows for more precise control over the pitching amplitudes. This method moves the model at a constant angular motion and the torque inputs required to generate the motion are used to calculate the damping. References 13 and 14 provide detailed descriptions of these two method for calculating pitch damping. It should be noted, however, that each approach actually determines the sum $C_{m\dot{\theta}} = C_{mq} + C_{m\dot{\alpha}}$. It is not possible to separate the two terms. It is also important to note that wind tunnels operate at a constant speed. However, as previously noted, the phugoid mode of a vehicle experiences wide variations in velocity. Therefore, for systems in which this mode dominates, it may be difficult or impossible to accurately obtain this information in the wind tunnel³².

Cabling systems such as those used for aeroelastic testing may be used for damping

derivatives, however, the resulting analysis is more complex than the oscillatory fixed sting testing. As an additional complexity to calculation of damping derivatives in the wind tunnel, most model suspension systems allow for freedom in pitch, yaw, and vertical translation, but are limited in other dimensions. This precludes the calculation of roll damping, which has been shown previously to be of most interest for many missile systems.

Aside from cost, there are other downsides to determining damping derivatives within the wind tunnel. While damping derivatives can be obtained through dynamic wind tunnel testing, typical dynamic experiments are focused on the dynamic behavior dominated by rigid body motions or aeroelastic effects³². As evidenced by the equations of motion, inertia matters for dynamic derivative computation. Typical wind tunnel test models are subscale to fit in a desired wind tunnel facility. For a static test, the model, typically fabricated from metal, is scaled in size, but weight and density are not considered. As long as Mach number and Reynolds number can be matched, the composition of the model is not considered beyond meeting the facility safety requirements. However, for dynamic testing, aerodynamic scaling must also be applied to the inertia and rotation rates. This can result in a substantially more complex and expensive model.

There is yet another problem with the use of wind tunnel testing. Until recently, all dynamic testing for damping derivatives was focused on the low speed regime due to the availability of mounting structures. As higher speeds show an increased need for damping accuracy, this is a problem that is currently being worked within the ground testing community. In particular, NASA Langley is updating their facilities to accommodate higher speed testing¹².

3.2.2 Aeroballistic Range Testing

Most of the historical damping data available was obtained through aeroballistic range or spark range testing^{5,9,10}. This technique is typically used for artillery rounds, most of which do not have fins. As a result, this data was extensively used in the development of body alone semi-empirical predictions. There is however, a very limited set up data for configurations with fins. These test ranges are free flight facilities that utilize high speed photography to capture the orientation of a projectile along its flight path¹⁰. Proper data

reduction requires accurate measurements of the angular orientation (both in roll and in pitch) and the linear position of the projectile. In order to obtain these measurements, shadowgraph images are taken at multiple discrete locations along the trajectory. In order to properly orient the fins, locator pins are often used so that they can be easily identified in the images. By examining the changes in the orientation of the missile at each photographic station, it is possible to determine the static and dynamic (i.e. damping) characteristics of the vehicle. Details of the data reduction process in use at these facilities can be found in references 9 and 10.

3.2.3 Computational Approaches

With the advent of faster computers, computational approaches appear to be replacing the use of spark ranges and wind tunnels for the determination of damping derivatives. Significant efforts have been invested to improve the capabilities and accuracies of the various computations¹⁵.

In its infancy, CFD was focused solely on attached flow and understanding the various flow fields. As computers and methods progressed, CFD began to analyze more complex flows and obtain force and moment coefficients for such flows. There are however, several challenges with respect the use of CFD for dynamic stability computations. Despite the accuracy and capability of the various computational approaches, the results are very computer resource intensive and may require long set-up and computation times. For a configuration that is late in its development cycle, this is often acceptable. However, for configurations that are early in the design phase or where the damping terms must be approximately known, faster methodologies are desired. Additionally, dynamic stability problems often present separated flows which can pose a problem for certain CFD codes. Often very high grid resolution is necessary in these regions to accurately capture the flow¹⁵. Regardless, significant work is being done for quasi steady flows that represent a reasonable prediction of the damping derivatives.

4 Sensitivity Analysis

One of the primary, and often most difficult, tasks for the engineer is to determine when a solution is “good enough”. This is particular true for damping derivatives as the methodologies for prediction are often very simple or very complex. The flows that generate the damping derivatives are complex, and as such, do not generally have a closed form solution. As such, the engineer must have some knowledge about which assumptions are acceptable and how the accuracy will affect the overall results. The idea of “good enough” may also be applicable to the background engineer. For some stability and control engineers, an answer of the approximate magnitude might be good enough. A computation expert however, might wish to have a complete understanding of the flow field and accuracy to tenths of a percent. Figure 7 presents a humorous illustration of this issue.

CFD'ers	S&C'ers
Flow physics	Forces & Moments
Incipient separation	Massive separation
Lift, Drag, L/D	6 components
Design point	Envelope & beyond
Symmetric flight	Alpha & beta
Static aircraft	6 DOF motions
1% accuracy	Plus or minus
Optimize	Cut & try
S&C-challenged	CFD-challenged

Figure 7. Engineering Accuracy Thoughts¹⁵

For practical missile design, accuracy requirements typically lie somewhere between

both of these schools of thought. To gain some insight into this problem, a sensitivity analysis is beneficial. Typically, such analysis is not conducted prior to the computation of complex derivatives. In such an analysis, the term of interest is set to a nominal value. For this study, values of C_{lp} , C_{mq} and/or $C_{m\dot{\alpha}}$ as calculated by a common aerodynamic prediction tool were used for the nominal value. This value is then varied from the nominal value and changes in the flight characteristics are noted.

There are several ways that a sensitivity analysis could be performed. Upon initial consideration, the use of a six degree of freedom (6-DOF) simulation appears to be the most obvious answer. Such a simulation would “virtually” fly the vehicle through a complete trajectory. The aerodynamic coefficients, including the damping terms, are obtained from tables as a function of orientation and velocity. The damping terms could be varied to determine the impact on range, time of flight, etc. While it appears this methodology would provide the most useful information, there are a few inherent limitations. In general, 6-DOF simulations for a guided vehicle are not generic. They are specifically designed for a given vehicle and a properly developed autopilot is used. Additionally, the control laws used in the autopilot are based on the aerodynamics provided. As a result, altering the aerodynamics in the tables would result in a situation where the autopilot was no longer properly tuned. It would be difficult to determine if changes in flight characteristics were the result of variations in the damping terms or the result of a poorly tuned autopilot.

Two additional options involve examining the equations of motion of a vehicle. The first methodology analyzes the equations and determines the change in acceleration due to varying values of the damping derivatives and/or angular rates (velocities). These equations allow for a quick, linear, analysis of variations in the damping terms. The alternate approach is to evaluate the stability matrices that are developed from the equations, as shown in Etkin.² These matrices provide information about the modes and are used for autopilot development. Variations to the damping terms provide information about changes in the damping ratio, natural frequencies, time-to-half, the period, and stability of a given flight mode. The analysis and results of these two approaches are provided in the following sections.

4.1 Acceleration Analysis

The acceleration analysis is really an analysis of the equations of motion. The damping terms are varied such that changes in the vehicle acceleration are determined. For this study, the equations 16-18 from Roskam³³ were utilized. The equations and assumptions applied to the analysis will be discussed in depth in the appropriate section, however, it is prudent to first examine the equations for the roll acceleration and the two pitch accelerations, as shown in equations 16-18, respectively.

$$I_{xx}\dot{p} - I_{xz}\dot{r} = QSd \left\{ C_{l\beta}\beta + C_{lp}\frac{pd}{2V} + C_{lr}\frac{rd}{2V} + \text{control terms} \right\} \quad (16)$$

$$I_{yy}\dot{q} = QSd \left\{ (C_{mu} + 2C_{m1})\frac{u}{V} + (C_{mtu} + 2C_{mt1})\frac{u}{V} + C_{m\alpha}\alpha + C_{m\alpha}\alpha + C_{m\alpha}\frac{\dot{\alpha}d}{2V} + C_{mq}\frac{qd}{2V} + \text{control terms} \right\} \quad (17)$$

$$m(\ddot{\alpha} - Vq) = -mg\theta \sin \theta + QS \left\{ -(C_{LU} + 2C_{L1}) - (C_{L\alpha} + C_{D1})\alpha - C_{L\dot{\alpha}}\frac{\dot{\alpha}d}{2V} - C_{Lq}\frac{qd}{2V} + \text{control terms} \right\} \quad (18)$$

Since the values of C_{mq} , $C_{m\dot{\alpha}}$, and C_{lp} are of interest to this work, it would stand to reason that the values of \dot{p} , $\ddot{\alpha}$, and \dot{q} would be of interest to this sensitivity study. However, upon examination of the equations of motion it is clear that $\ddot{\alpha}$ is a function of the force derivatives and not the desired moment derivatives. However, the effect of $C_{m\alpha}$ on the pitching acceleration is still examined.

For this analysis, a generic missile configuration was examined. The configuration is often referred to as the Army-Navy finner. This configuration was chosen as there is a significant amount of damping derivative data available in open literature³⁴⁻³⁹. The configuration, shown in Figure 8, consists of a basic 10 caliber body with a 2 caliber conical nose and a 4 fins located with the fins aligned at the base of the body. The fins are square in planform with a 1 caliber root chord, tip chord and exposed semi-span.

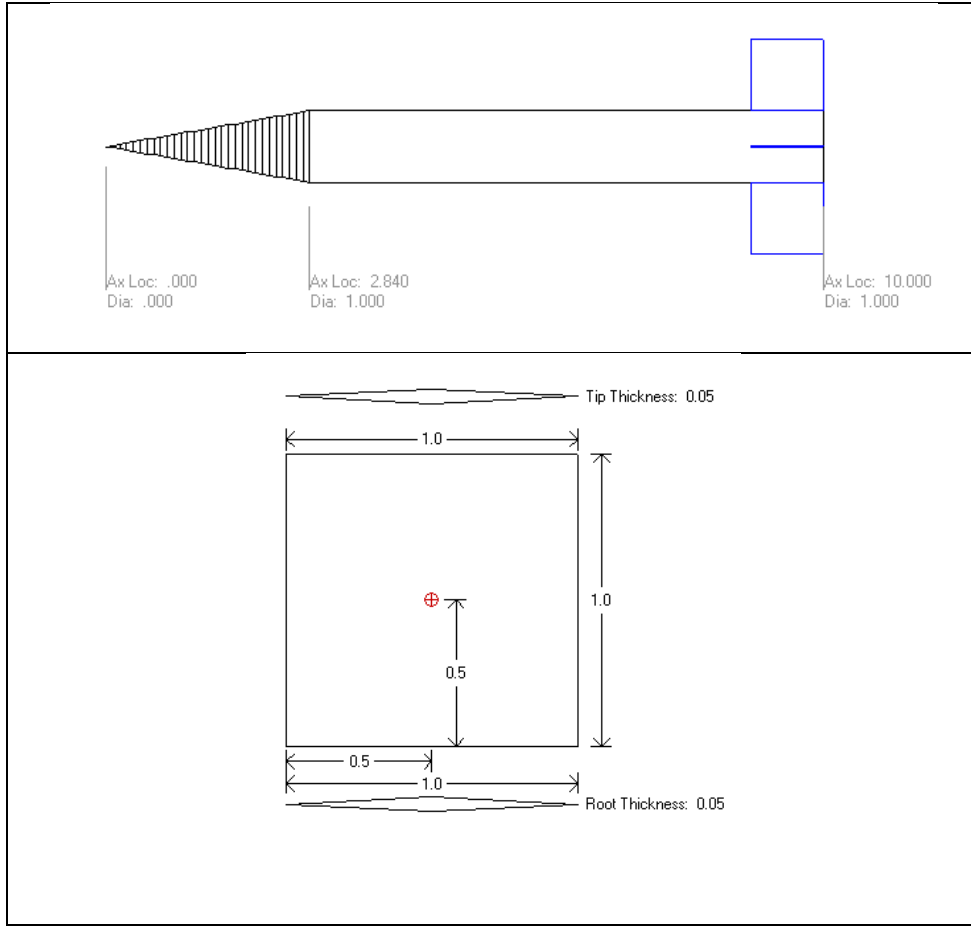


Figure 8. Basic Finner Configuration

4.1.1 Lateral Analysis

For the purpose of this analysis, a simplified solution of equation 16 neglecting the control terms will be utilized. For the fully symmetric configuration considered in this analysis, the values of I_{xz} is neglected. The problem could also be approached assuming that the vehicle is in pure roll with no yaw rates present, which would also drop the I_{xz} term. Furthermore, for this analysis, the sideslip angle and yaw rate are assumed to be zero. This leads to equations 19 and 20.

$$I_{xx}\dot{p} = Q S d \left\{ C_{lp} \frac{pd}{2V} \right\} \quad (19)$$

$$\dot{p} = \frac{Qsd}{I_{xx}} \left\{ C_{lp} \frac{pd}{2V} \right\} \quad (20)$$

From these simplified equations, it is quite evident that the roll acceleration (or deceleration for a stable system) is depended on the vehicle size (d , S , and I_{xx}) and flight conditions (V , Q , and p). For this analysis, the values of roll rate and Mach number (velocity) are varied for a range of C_{lp} values for the basic finner. The actual Missile Datcom⁶ predicted values of C_{lp} are shown in Table 1. The value of I_{xx} obtained from literature^{5,36,39} is 0.0098 slug-ft².

Table 1. Missile Datcom Predicted Values of C_{lp}

Mach	C_{lp} (per radian)
M=0.25	-25.9
M=0.5	-26.8
M=0.8	-28.7
M=1.25	-35.1
M=2.0	-19.6

Figure 9 shows the variation in \dot{p} with variations in C_{lp} , and Mach number. Examining the equation, this result is quite obvious as the roll rate is simply a multiplier to the slope. Thus, the slope for a 3Hz roll rate will be exactly 3 times the slope for a 1 Hz roll rate. As a result, only a nominal 3 Hz limit is displayed. For the purposes of this analysis, the variations in CLP represent the accuracy with which the value is predicted. As previously noted, except for rare cases, the values of a C_{lp} for a finned body will always be negative, or stable². In other words, motion will be damped, not amplified. This is evident from the negative (or decelerating) values of \dot{p} . At low Mach numbers the vehicle is relatively insensitive to the roll damping values. That is the roll deceleration does not vary significantly with changes in the roll damping coefficient. For the case of Mach 0.25 and a 1 Hz roll rate, the slope of the line is 0.00294, or nearly zero. In contrast, as Mach number increases, the value of \dot{p} becomes more sensitive to the C_{lp} accuracy. At Mach 2

and 1 Hz, the slope of the line is 0.2361, considerably higher than at Mach 0.25. Additionally, as roll rate increases the vehicle sensitivity to C_{lp} accuracy increases.

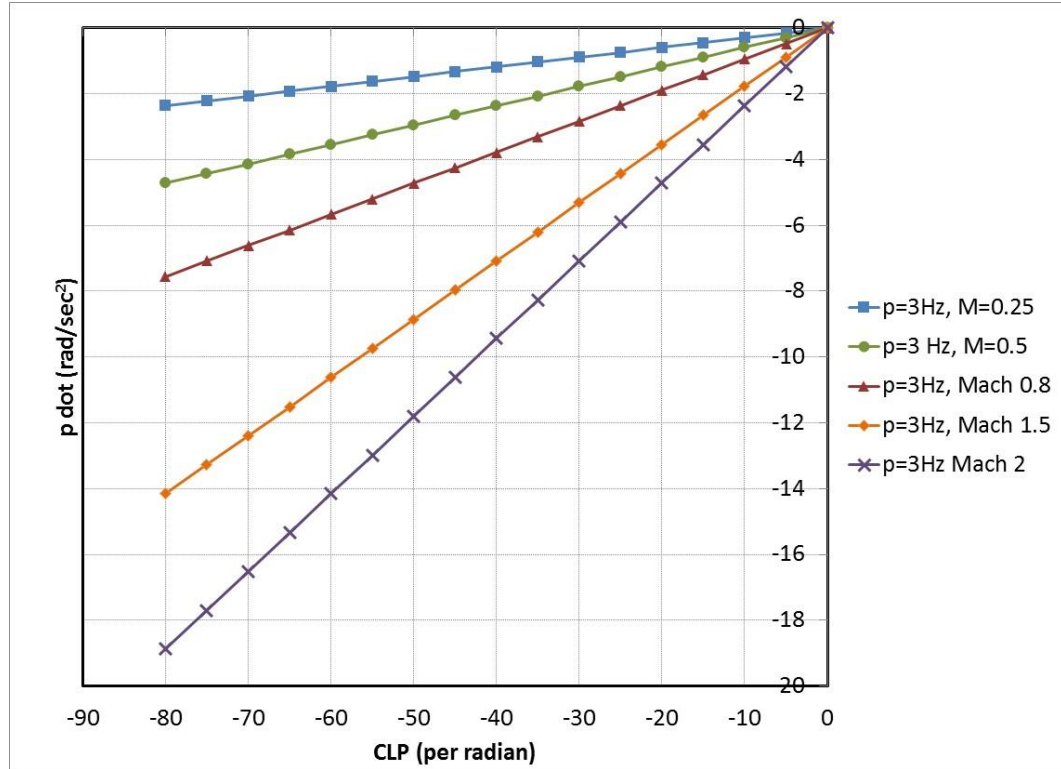


Figure 9. Roll Deceleration Variation with C_{LP}

As an added exercise, the inertia was varied while the C_{lp} value was held at the Datcom prediction. These results are shown in Figure 10. Due to I_{xx} appearing in the denominator of the equation, as the inertia is reduced, the roll acceleration begins to increase rapidly. What is of note is that there is a substantial effect of inertia on the roll acceleration of the system.

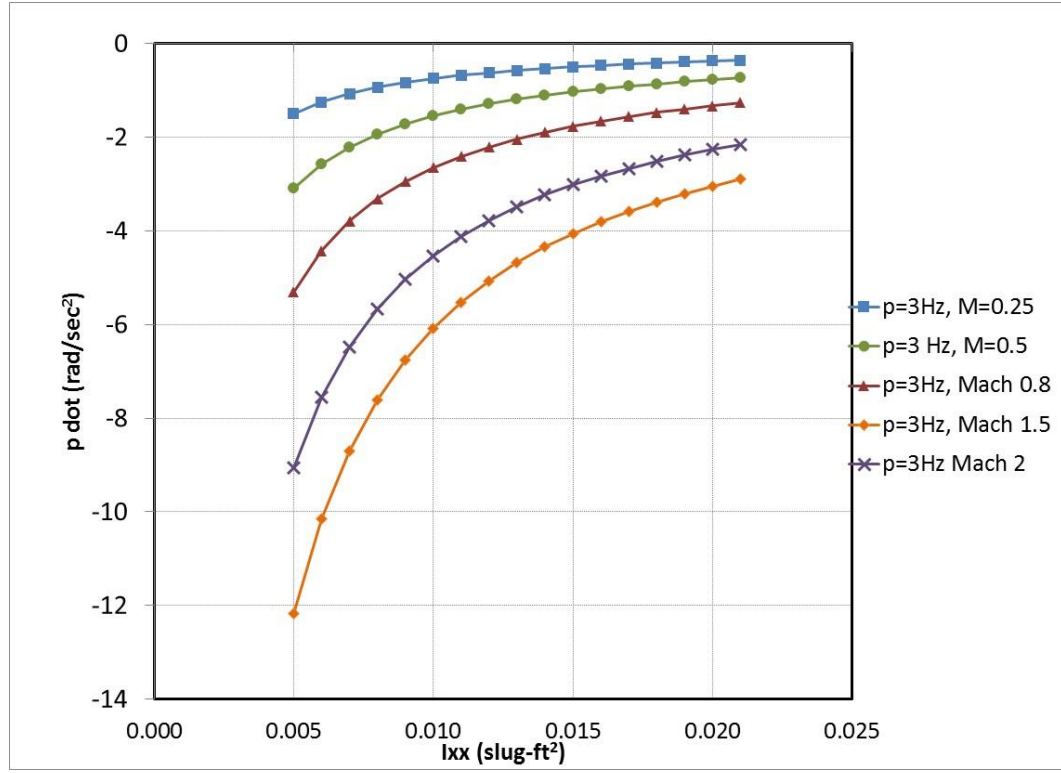


Figure 10. Roll Deceleration Variation with Ixx

These results are important as they indicate how much effort is required to obtain the values of C_{lp} . At low Mach numbers and low roll rates where the vehicle is relatively insensitive to C_{lp} , a full CFD solution might not be required and lower order methods are sufficient. However, as Mach number increases, increased fidelity methods used to calculate C_{lp} might become necessary as accuracy is more important. Of additional importance is the inertia of the vehicle. For very low inertia systems, particularly those flying at high Mach numbers, the vehicle may be very sensitive to roll damping accuracy and as such more thorough analysis should be performed.

4.1.2 Longitudinal Analysis

As previously presented, the pitching equation is shown in equation 17. The $\ddot{\alpha}$ equation is not presented as it is not a direct function of the C_{mq} and $C_{m\dot{\alpha}}$ that are desired. However, both q and $\dot{\alpha}$ effect the pitch acceleration/deceleration term, \dot{q} .

As with the roll equation, some simplifying assumptions are made for the pitch equation. The control terms are again neglected, the thrust terms are neglected and the u velocity is assumed to be negligibly small. These assumptions result in the following equations.

$$I_{yy}\dot{q} = QSD \left\{ C_{m\alpha}\alpha + C_{m\dot{\alpha}} \frac{\dot{\alpha}d}{2V} + C_{mq} \frac{qd}{2V} \right\} \quad (21)$$

$$\dot{q} = \frac{QSD}{I_{yy}} \left\{ C_{m\alpha}\alpha + C_{m\dot{\alpha}} \frac{\dot{\alpha}d}{2V} + C_{mq} \frac{qd}{2V} \right\} \quad (22)$$

In the case of the pitch equation, it is more difficult to isolate the individual effects of the damping terms as most aircraft fly with a slight angle of attack. As such, a small, 2 degree angle of attack is considered for this analysis. Additionally, a nominal 0.1 Hz pitch rate will be considered when $\dot{\alpha}$ is varied, and conversely, a nominal 0.1 Hz angle of attack rate is considered when q is varied. This is still a linear equation of the form $y=mx+b$. The damping term under consideration and the angular rate for that term drive the slope of the line. Keeping the values of $C_{m\alpha}$ and the other damping term constant will merely effect the intercept value.

As with the roll damping analysis, the basic finner configuration was utilized with this analysis. Table 2 provides the Missile Datcom⁶ predicted aerodynamic coefficients. The inertia, I_{yy} , was found to be 0.00294 slug-ft² in the available literature^{5,36,29}.

Table 2. Missile Datcom Longitudinal Predictions

Mach	$C_{m\alpha}$	$C_{m\dot{\alpha}}$	C_{mq}
0.25	-24.735	-32.276	-277.3
0.5	-25.887	-30.7	-289.918
0.8	-29.5	-28.739	-318.145
1.25	-39.138	-18.224	-464.669
2.0	-11.75	-13.47	-304.992

Figures 11 and 12 illustrate the effect of C_{mq} and $C_{m\dot{\alpha}}$ accuracy on the pitch deceleration. As is obviously expected, the results are linear with the slope being driven

by the Mach number and pitch rate, q . As with the roll rate, the value of q is just a multiplier to the slope so that a rate of 3 Hz produces a slope 3 times higher than a rate of 1 Hz. Also as with the roll rate, the sensitivity to variations in C_{mq} and $C_{m\dot{\alpha}}$ increase with increasing Mach number. The system appears much more sensitive to variations in C_{mq} than in $C_{m\dot{\alpha}}$; however, further examination is needed before drawing conclusions. Since the same rates are used for q and $\dot{\alpha}$, the slopes of the two lines are actually the same. However, Predicted values of $C_{m\dot{\alpha}}$ are typically much smaller than values of C_{mq} , which leads to inherently smaller rates of \dot{q} . If the same range of damping values were utilized for C_{mq} and $C_{m\dot{\alpha}}$ there would be much more similarity in the results. However, due to its larger value, C_{mq} accuracy will likely have a much larger impact on a system than $C_{m\dot{\alpha}}$ accuracy.

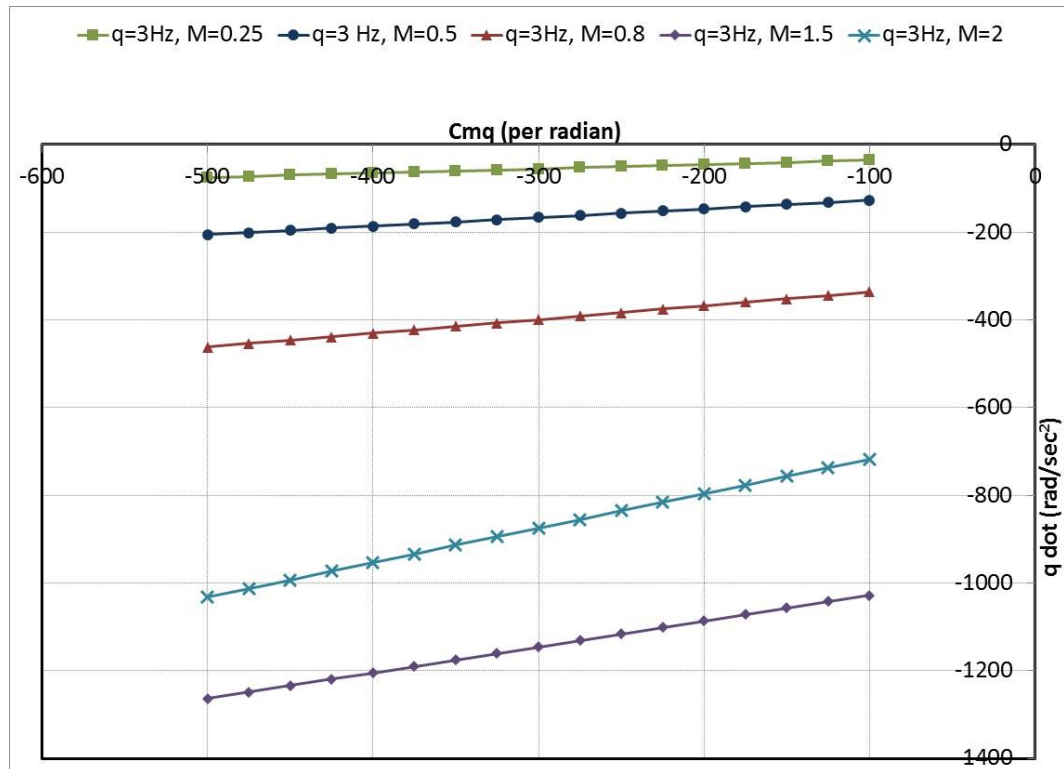


Figure 11. \dot{q} Variations with C_{mq}

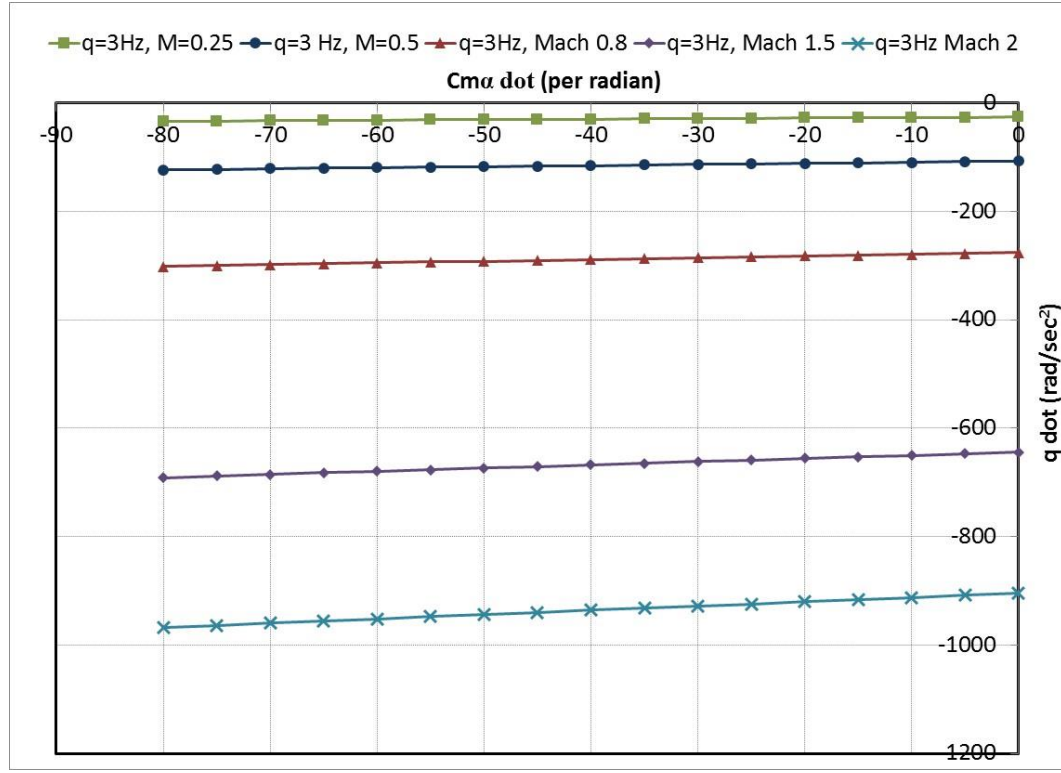


Figure 12. \dot{q} Variations with $C_{m\dot{\alpha}}$

As with the roll damping, the effects of inertia were also considered by varying the system inertia while maintaining constant damping derivative values. As expected, the lower the inertia values, the more sensitive the system will be to pitch damping. This fact would be increasingly important to flying wing type designs where the inertia is typically small in relation to longer vehicles. These results are illustrated in Figure 13.

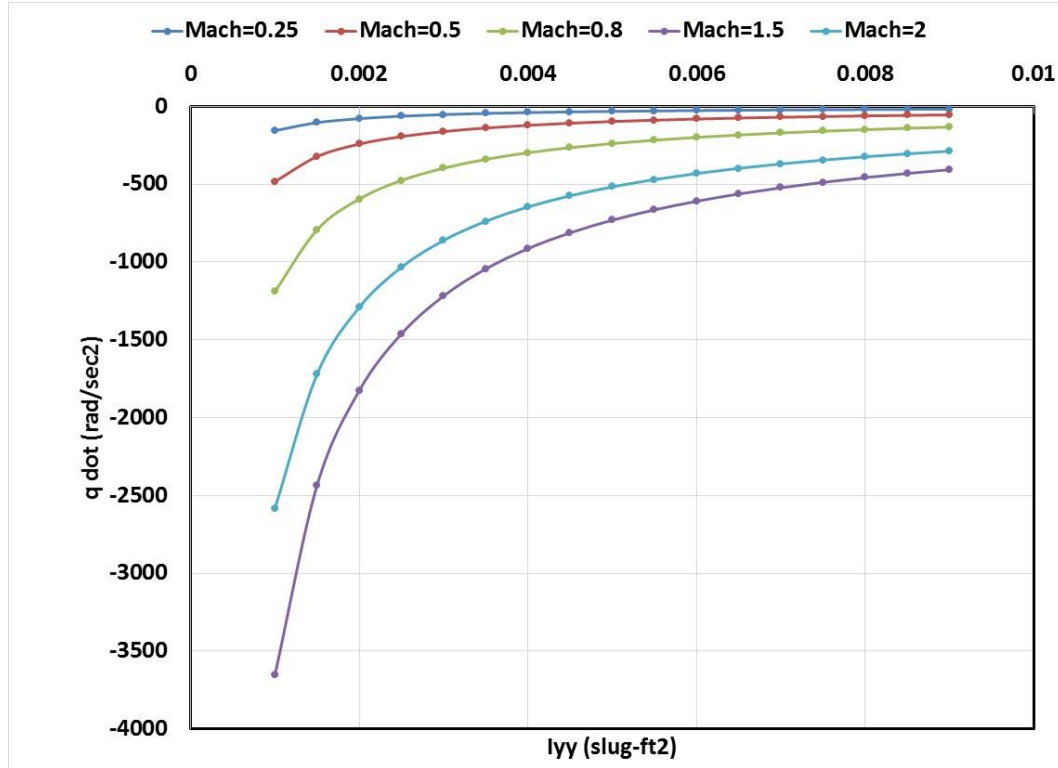


Figure 13. \dot{q} Variations with Inertia

4.2 Stability Mode Analysis

The results of the previous section give an overall idea about the effects of stability derivative accuracy, but they do not provide a complete picture. Clearly, the equations do contain all of the aerodynamic properties of the configuration. By undertaking an examination of the stability modes, more insight can be gained into the sensitivity of a system to the dynamic derivatives. The effect of a given derivative on the stability of a system be determined by analyzing the undamped natural frequency (ω_n), damping ratios (ζ), and/or time properties (time to half or double) of a system as a function of varying values of the selected stability derivative. The vales of ω_n , ζ , and time to half (or double) are calculated through an eigenvalue analysis of the appropriate stability matrix. The derivation of the matrices used for this analysis is found in Etkin², with the lateral and longitudinal matrices given in the following equations. Note that for this analysis, a controls-free approach was taken to simplify the analysis.

The lateral state equation is shown in equation 23 in matrix form. An eigenvalue analysis of the stability matrix results in three modes of motion for a typical system. These modes are the dutch roll mode, the spiral mode, and the rolling mode. The dutch roll mode is oscillatory motion consisting of roll and yaw coupling. The other two modes are non-oscillatory in nature which the spiral mode characterized by yawing at negligible sideslip and the rolling mode characterized by rotation about the longitudinal axis. A complete definition of these modes is provided in Etkin² or Roskam³³.

$$\begin{bmatrix} \Delta\dot{\beta} \\ \Delta\dot{p} \\ \Delta\dot{r} \\ \Delta\dot{\phi} \\ \Delta\dot{\psi} \end{bmatrix} = \begin{bmatrix} \frac{Y_v}{m} & \frac{Y_p}{m} \frac{2}{b} & \frac{Y_r - u_o}{m} \frac{2}{b} & g \cos \Theta_o / u_o & 0 \\ \left(\frac{L_v}{I_{xp}} + I_{xzp} L_p \right) \frac{b}{2} & \frac{L_p}{I_{xp}} + I_{xzp} L_p & \frac{L_r}{I_{xp}} + I_{xzp} L_r & 0 & 0 \\ \left(\frac{N_v}{I_{xp}} + I_{xzp} L_p \right) \frac{b}{2} & \frac{N_p}{I_{xp}} + I_{xzp} L_p & \frac{N_r}{I_{xp}} + I_{xzp} L_r & 0 & 0 \\ 0 & \frac{2u_o}{b} & \frac{2u_o \tan \Theta_o}{b} & 0 & 0 \\ 0 & 0 & \frac{2u_o}{b \cos \Theta_o} & 0 & 0 \end{bmatrix} \begin{bmatrix} \Delta\beta \\ \Delta\hat{p} \\ \Delta\hat{r} \\ \Delta\phi \\ \Delta\psi \end{bmatrix} \quad (23)$$

The longitudinal state equation is shown in equation 24 in matrix form. For most systems, two modes result from the analysis of the longitudinal state matrix. The first mode is the phugoid mode. This mode is characterized by a near constant pitch angle with changes in speed. The second mode is the short period mode, which is characterized by constant speed and rapid pitch changes.

Etkin² offers a simplification for the longitudinal analysis. Within this simplification, the pitch damping terms do not affect the phugoid mode. This is in line with results from other references. Instead, C_{mq} and $C_{m\dot{\alpha}}$ affect only the short period mode. As such, the longitudinal state matrix can be reduced to the following

$$\begin{bmatrix} \dot{w} \\ \dot{q} \end{bmatrix} = \begin{bmatrix} \frac{z_\alpha}{m} & u_0 \\ \frac{1}{I_{yy}} \left[M_\alpha + \frac{M_{\dot{\alpha}} z_\alpha}{m} \right] & \frac{1}{I_{yy}} \left[M_q + M_{\dot{\alpha}} u_o \right] \end{bmatrix} \begin{bmatrix} w \\ q \end{bmatrix} \quad (24)$$

The analysis simplifies to equations 25 through 31 to determine the eigenvalues.

$$\lambda^2 + B\lambda + C = 0 \quad (25)$$

$$B = -\frac{1}{t^*} \left[\frac{C_{z\alpha}}{2\mu} + \frac{1}{I_y} (C_{mq} + C_{m\dot{\alpha}}) \right] \quad (26)$$

$$C = -\frac{1}{t^{*2} I_y} \left(C_{m\alpha} - \frac{C_{mq} C_{z\alpha}}{2\mu} \right) \quad (27)$$

$$t^* = \frac{c}{2u_0} \quad (28)$$

$$\mu = \frac{m}{\frac{1}{2}\rho Sc} \quad (29)$$

$$\hat{I}_y = \frac{I_{yy}}{\rho S \left(\frac{1}{2}c\right)^3} \quad (30)$$

$$C_{z\alpha} = -C_{N\alpha} \quad (31)$$

For each analysis (lateral and longitudinal) the eigenvalues, λ , are computed using a simple computer script. Then, for each mode (short period for longitudinal stability, rolling, spiral and dutch roll for lateral stability) the values of ω_n , ζ , and time to half (or double) are computed from equations 32 through 35.

$$\lambda = n \pm i\omega \quad (32)$$

$$\omega_n = (\omega^2 + n^2)^{1/2} \quad (33)$$

$$\zeta = -\frac{n}{\omega_n} \quad (34)$$

$$t_{half} \text{ or } t_{double} = \frac{0.693}{|n|} \quad (35)$$

The eigenvalues for each mode are used to develop transfer functions. By definition, a transfer function is the ratio of output to inputs of a linear system and is expressed in the LaPlace transform variable, s. The transfer functions are used in autopilot development to

determine the dynamic response characteristics of a system together with the associated control system and autopilot. For oscillatory modes, the transfer functions take on the form shown in equation 36.

$$\frac{K}{s^2 + 2\zeta\omega_n s + \omega_n^2} \quad (36)$$

In the above equation, the gain is defined by K/ω_n^2 and the transfer function is the denominator². It is in this capacity that the sensitivity to the damping derivative accuracy becomes apparent.

For non-oscillatory modes, such as those typically seen in the lateral stability analysis, there is clearly no natural frequency to measure. In the case of these modes, it is the time constant, T, that is of primary interest^{2,23}. This value is defined as the negative inverse of the corresponding eigenvalue and is a measure of how quickly the system responds to an input. A smaller time constant will respond faster to a given disturbance. In other words, a heavily damped system should have a very low time constant. Again, the basic finner missile was used as a test case due to the amount of data available in the literature.

4.2.1 Lateral Stability Analysis of a Generic Missile

As previously mentioned, the generic configuration analyzed for this sensitivity study was the basic finner missile. Unlike with the acceleration analysis, a considerable amount of aerodynamic data is needed to perform the complete matrix analysis of the airframe. These aerodynamic coefficients were obtained from Missile Datcom. Table 3 lists the aerodynamic coefficients used for the analysis.

Table 3. Lateral Aerodynamics of the Basic Finner

Mach	$C_{l\beta}$	C_{lp}	C_{lr}	$C_{n\beta}$	C_{np}	C_{nr}	$C_{y\beta}$	C_{yp}	C_{yr}
0.25	0.0	-25.9	0.0	30.573	0.0	-361.8	-12.7683	0.0	106.0
0.5	0.0	-26.8	0.0	31.91	0.0	-374.6	-13.1186	0.0	107.4
0.8	0.0	-28.7	0.0	36.24	0.0	-408.2	-14.3481	0.0	116.16
1.25	0.0	-35.1	0.0	47.67	0.0	-575.5	-17.2151	0.0	143.181
2.0	0.0	-19.6	0.0	17.19	0.0	-364.4	-10.6225	0.0	88.819

Analysis of the lateral stability matrix showed no variation on the dutch roll or spiral modes of the vehicle. This trend resembles results in literature that indicate the C_{lp} will have a noticeable impact on the rolling mode only^{2,23}. The rolling mode time constant for variations in C_{lp} are shown in figure 14. As C_{lp} decreases toward 0 (i.e. no damping), the time constant begins to increase exponentially. The plots have been limited to a C_{lp} of -10 in order to permit easier visual analysis. The system is most sensitive at low Mach numbers, as evidenced by the larger variations in time constant at the lower Mach numbers. At Mach 0.25, a deviation of 20 percent in the predicted C_{lp} can result in a 10 second change in the time constant. At Mach 0.5, the same deviation results in an approximate 8 second change, while at Mach 2 the difference is on the order of 2 seconds.

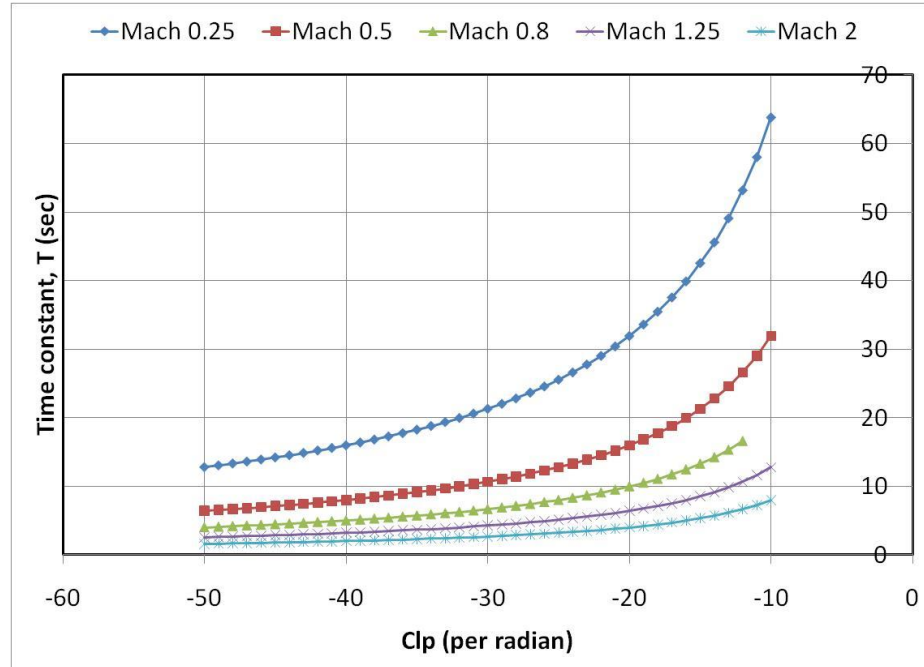


Figure 14. Basic Finner Rolling Mode Time Constant Variation with C_{lp}

4.2.2 Longitudinal Stability Analysis of a Generic Missile

The aerodynamic properties used to conduct the analysis of the basic finner are shown in table 4. These are identical to the values used in the previous linear analysis, with the addition of $C_{L\alpha}$ and C_{D0} , which are necessary to complete the short period stability matrix analysis.

Table 4. Basic Finner Longitudinal Aerodynamics

Mach	$C_{m\alpha}$	$C_{m\dot{\alpha}}$	C_{mq}	$C_{L\alpha}$	C_{D0}
0.25	-24.735	-32.276	-277.3	12.925	0.228
0.5	-25.887	-30.7	-289.918	13.269	0.1991
0.8	-29.500	-28.739	-318.145	14.467	0.2375
1.25	-39.138	-18.224	-464.669	17.283	0.5641
2.0	-11.75	-13.47	-304.992	10.5908	0.4127

Figures 15 and 16 indicate that there is essentially no variation in the short period mode characteristics with variations in C_{mq} for this configuration. There is slight variation in the damping ratio resulting from the variation in the damping term, but overall, this is a very small change and has no appreciable effect on any of the periodic qualities of the mode.

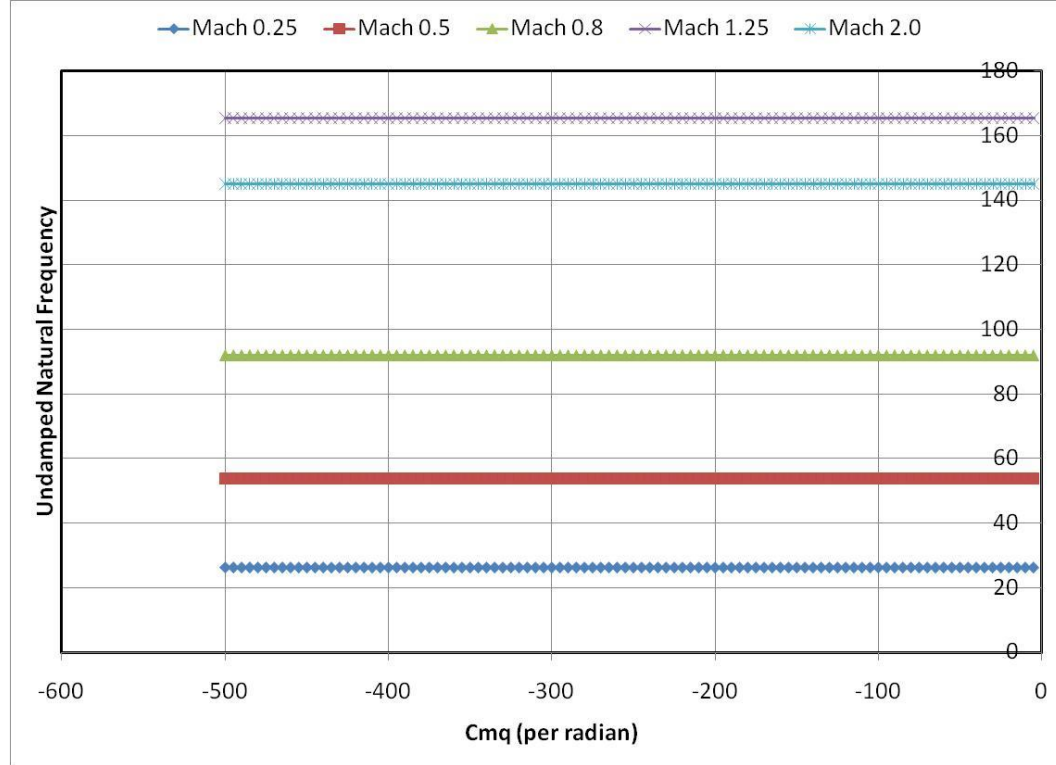


Figure 15. Undamped Natural Frequency Variation with C_{mq}

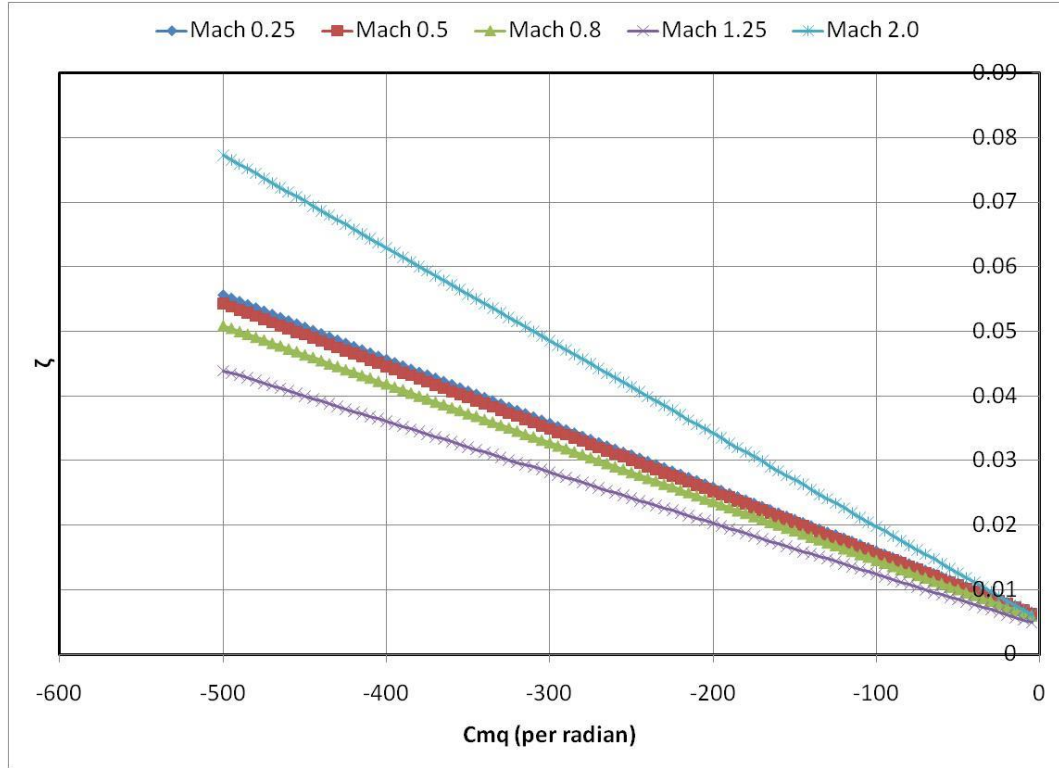


Figure 16. Damping Ratio Variation with C_{mq}

The results of varying $C_{m\dot{\alpha}}$ for this configuration are shown in figures 17 and 18. As with the C_{mq} variations, the changes are negligible. The damping ratio shows even less variation than what was noted with changing C_{mq} . This effect is to be expected if the short period equations are examined closely. The $C_{m\dot{\alpha}}$ term appears only as an additive value to C_{mq} . The C_{mq} term however, appears as a single term in the matrix. This coupled with the fact that $C_{m\dot{\alpha}}$ is approximately an order of magnitude smaller than C_{mq} leads to the reasonable conclusion that $C_{m\dot{\alpha}}$ should have less of an effect on the mode characteristics than C_{mq} .

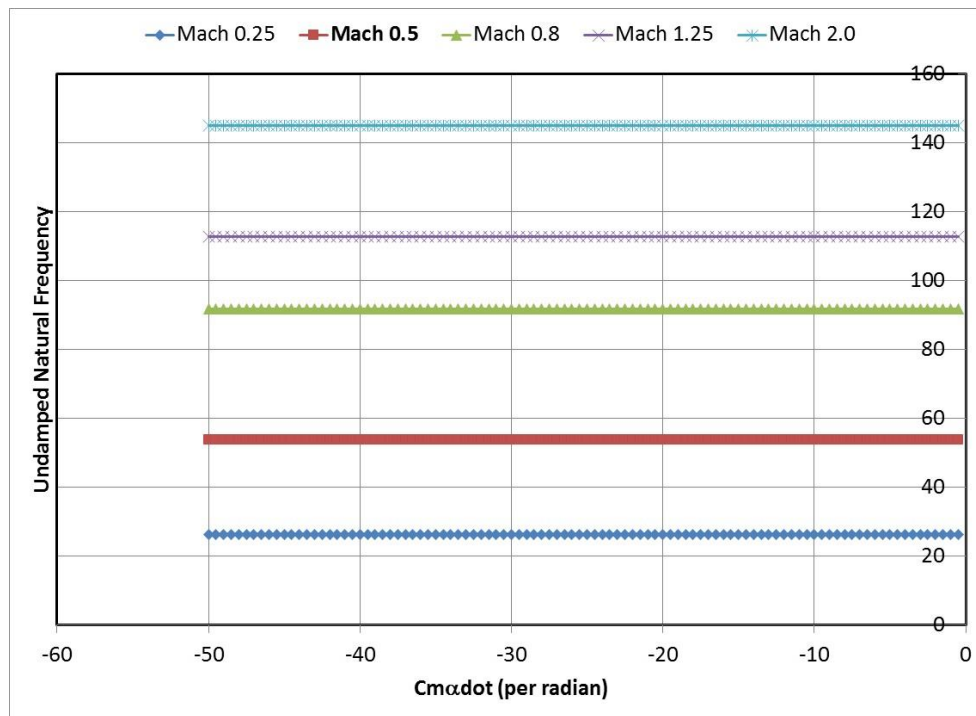


Figure 17. Undamped Natural Frequency Variation with $C_{m\dot{\alpha}}$

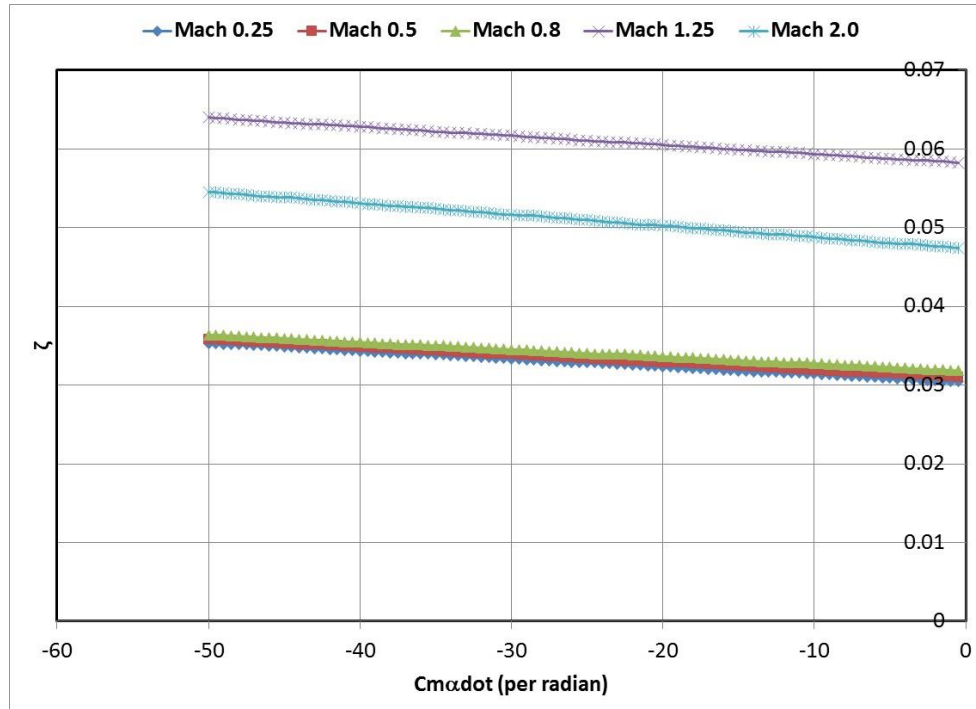


Figure 18. Damping Ratio Variation with $C_{m\dot{\alpha}}$

It should be noted that the results presented in this section apply only to the missile configuration presented. As such, it may be difficult to generalize the significance of the results. It is also noted that this configuration consists only of a body and an aft mounted tail. These facts make it a highly stable configuration, and as such, it is expected to be heavily damped in the pitch plane. One would expect that a more unstable configuration or one with less inertia in the pitch plane would exhibit more sensitivity to accuracies in pitch damping. However, the results presented in this section indicate that a sensitivity analysis performed prior to the calculation of the damping derivatives can drive the engineer to a suitable prediction code. A high fidelity CFD code is simply not necessary for the computation of a value that has minimal impact on the overall performance of a system.

The results in this section also confirm the need for methodologies to compute the damping characteristics of a variety of configurations. The exact importance of a given derivative is highly configuration dependent as evidenced by the effects of inertia on the basic finner system. It should also be noted that the analysis done in this section focused on a One Factor at a Time (OFAT) sensitivity analysis. This approach is computationally fast and gives a good overview of the relative sensitivities. However, it does not provide a complete analysis of all interactions. To obtain this information, a complete design of experiments (DOE) approach would be valuable but is outside the scope of this effort.

5 Development of Prediction Methods

This section describes the methodologies developed within this work to predict the pitch and roll damping characteristics of arbitrary flight vehicle configurations. This work represents novel approaches to the currently available techniques in order to expeditiously calculate the damping derivative terms while maintaining or increasing accuracy of the currently available semi-empirical or theoretical approaches.

5.1 Modified Slender Body Theory

The work of Ericsson⁴⁰⁻⁴³ has been fundamental in understanding the longitudinal damping terms. Most of his work was centered on developing a rapid method for computing the pitch damping on both ballistic missiles and the Space Shuttle Orbiter. Ericsson uses a body build-up type approach whereby the body and fins may be analyzed separately if so desired. The approach he uses is also tailored to the speed regime in which he is operating. Several of his approaches centered on modifying slender body theory and this work further expands slender body theory.

The method presented in this section develops another version of modified slender body theory. In calculating the body pitch damping at subsonic Mach numbers, Ericsson utilized a modified form of slender wing (or body theory) to account for variations in Mach number. As it was developed from a delta wing configuration, it was titled slender wing theory in various references^{43,43}. In practice, the method derived by Bryson²⁶ is applicable to both slender wings and bodies, thus the terms may be used interchangeably. The method described in the following section further improves the overall development of the method.

5.1.1 Development of Mach Correlation

Per slender wing theory the pitch damping sum can be defined as in equation 37.^{25,42,43}

$$C_{m\dot{\theta}} = -2C_{N\alpha} \cos\alpha \left(\frac{l}{D}\right)^2 \left(\sqrt{K_m} - \frac{x_{cg}}{l}\right)^2 \quad (37)$$

Again, a factor of two is added to account for proper normalization. The term K_M is a Mach correction factor that is empirically derived. If K_M is equal to 1, the results of Bryson would be obtained. The slender body $C_{N\alpha}$ must also be modified with this Mach correction factor. Rewriting the above equation with the sonic value of $C_{N\alpha}$ yields the results in equations 38 and 39.

$$C_{N\alpha} = K_m(C_{N\alpha})_{SB} = 2K_m \quad (38)$$

$$C_{m\dot{\theta}} = -4K_m \cos\alpha \left(\frac{l}{D}\right)^2 \left(\sqrt{K_m} - \frac{x_{cg}}{l}\right)^2 \quad (39)$$

The term K_m is empirically derived from body alone data. In equation 40, Ericsson derived the subsonic correlation to be⁴³

$$K_m = (1 - 0.23\beta^2) \quad (40)$$

There was no information provided on the lengths or characteristics of the bodies used to derive this correlation.

Equation 40 is valid only for subsonic Mach numbers. However, slender body theory is actually Mach number independent as seen in previous sections. It stands to reason, then, that an empirical correlation could be developed for supersonic flow in much the same way as Ericsson's subsonic approach. Equation 41 was used as a starting point for the methodology developed in this work.

$$\begin{aligned} C_{m\dot{\theta}} &= -2(C_{N\alpha})_{SB} K_m K_E \cos\alpha \left(\frac{l}{D}\right)^2 \left(\sqrt{K_m} - \frac{x_{cg}}{l}\right)^2 = \\ &= -4K_m K_E \cos\alpha \left(\frac{l}{D}\right)^2 \left(\sqrt{K_m} - \frac{x_{cg}}{l}\right)^2 \end{aligned} \quad (41)$$

The Mach correlation factor needed to be derived from available supersonic body alone data. To derive the supersonic correlation, experimental data on a variety of bodies of revolution was used⁴⁴. This database contains wind tunnel data of various circular

bodies at subsonic and supersonic Mach numbers and is more extensive than the data used in previous efforts. To obtain the correlation, the value of C_{na} was calculated for bodies of varying length and nose shape as a function of Mach number as shown in Figures 19 and 20. The data for each body was curve fit so that the value at $\beta=0$ (or $M=1$) was 2 to satisfy the slender body theory requirements.

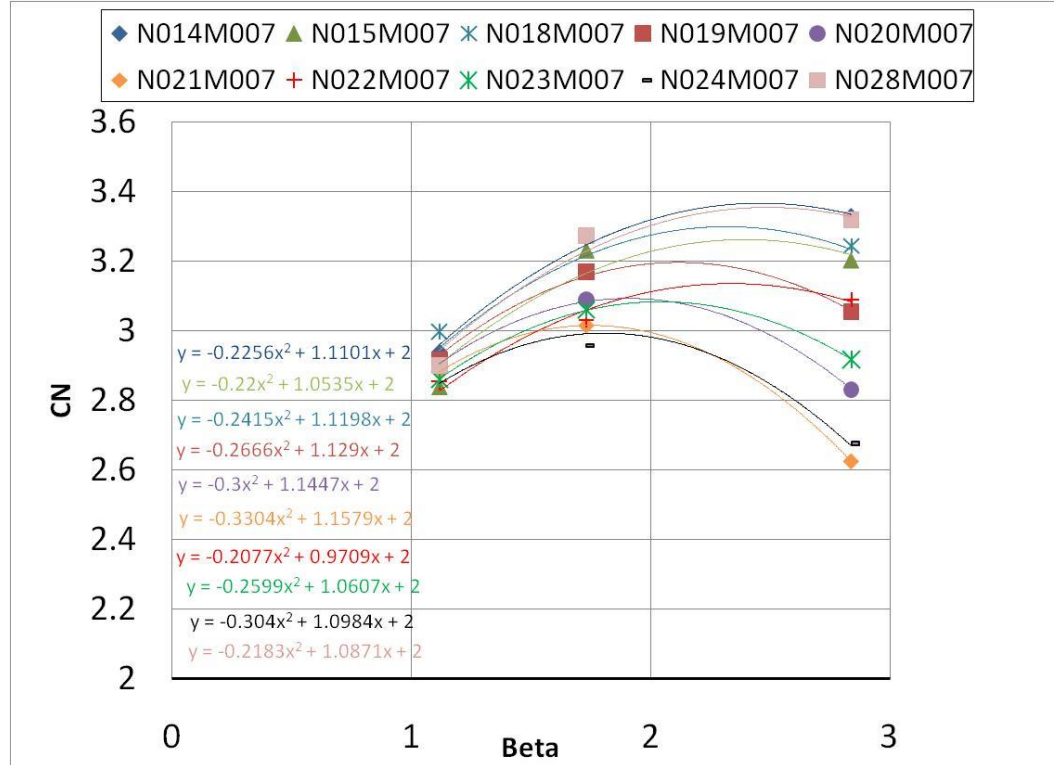


Figure 19.7 Caliber Centerbody Curve Fits

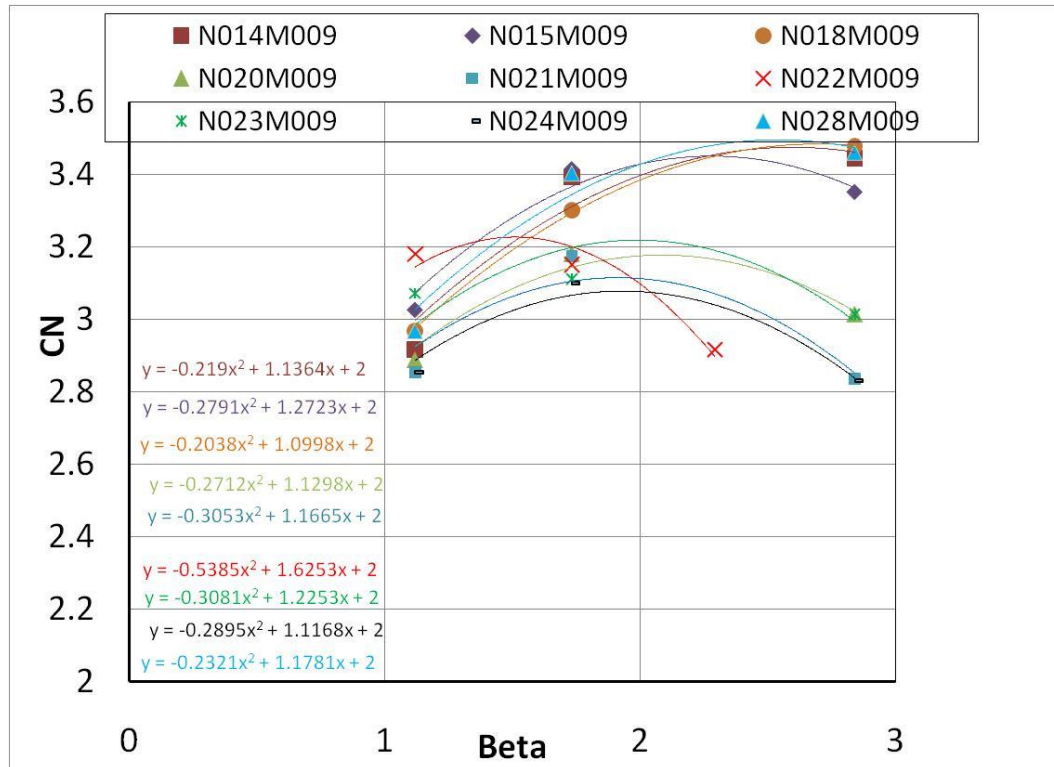


Figure 20.9 Caliber Centerbody Curve Fits

In the above analysis, Mach number was limited to 3. As higher Mach numbers were included, it was increasingly difficult to obtain reasonable curve fits. This observed Mach limit appears to fall in line with Ericsson's analysis that stated the slender wing Mach number limit was approximately 2.8⁴⁰⁻⁴³. Averaging all of the equations above, with the removal of the maximum presented value, the following correlation is determined.

$$K_m = -0.13006\beta^2 + 0.5627\beta + 1 \quad (42)$$

5.1.2 Development of Empirical Correlation

As all but the basic slender body theory (Bryson's approach) are semi-empirical in nature it is not unrealistic that a correction factor would be required with the current modified approach. For this work, an empirical correction factor, KE, was included in equation 41 as a possible means for improving the results from this method. By using

equations 41 and 42 to calculate $C_{m\dot{\theta}}$ for several configurations, it was determined that a correction factor of 0.5 yielded the best results. Figure 21 shows an example 7 caliber body with multiple correction factors applied at several CG locations.

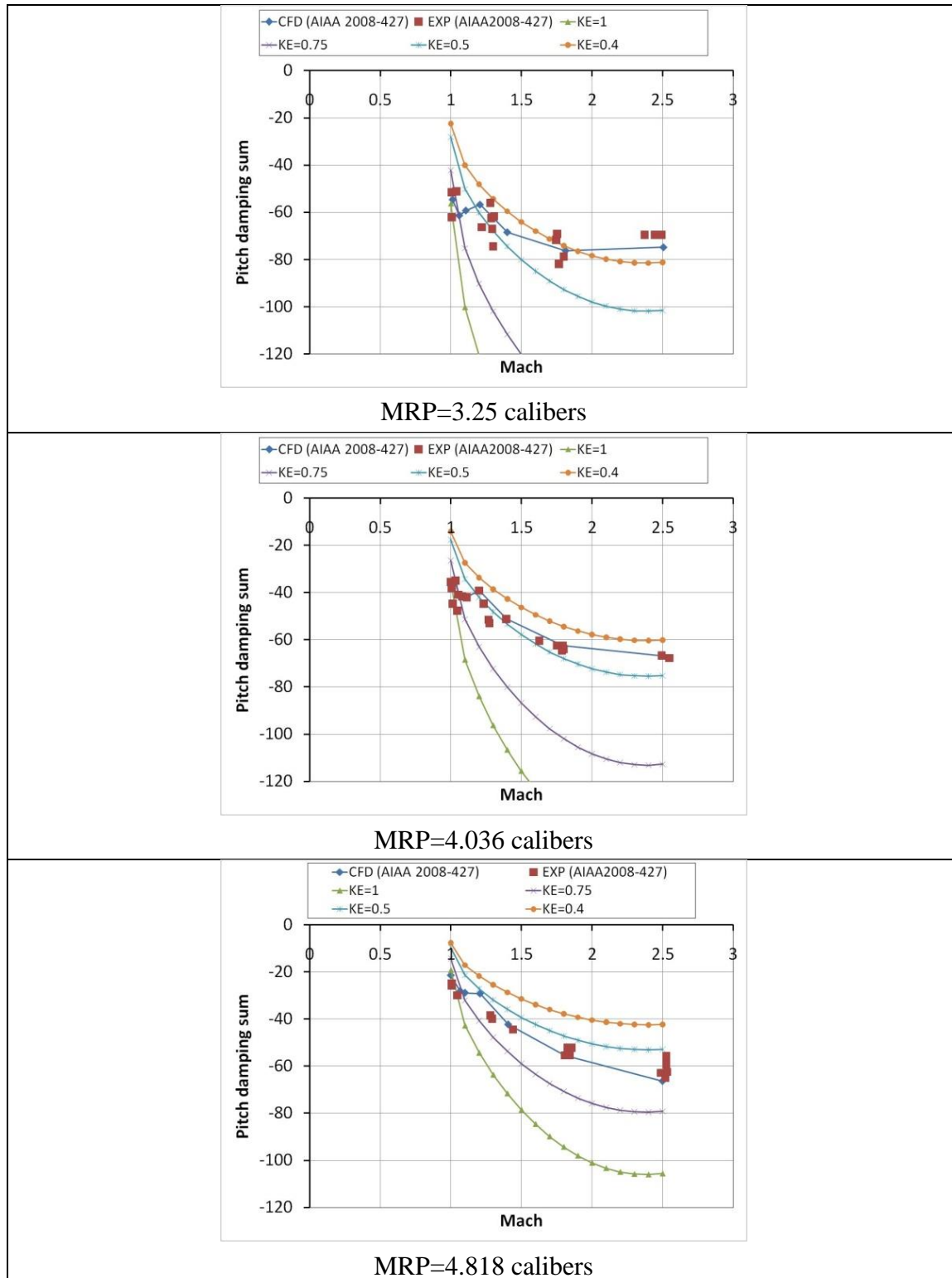


Figure 21. KE Values Determined from a 7 Caliber Body

From Figure 21, it is clear that the results are sensitive to shifts in the CG location. More explicitly, the sensitivity appears to be to the distance between the body volume centroid and the CG. This appears consistent with the derivation of the individual pitch damping terms in the ESDU reference⁴⁵. In that derivation, both terms contain the difference, $X_{vc} - X_{cg}$, although the term drops when the sum is calculated. While a correction factor of 0.5 appears to be a good compromise amongst the data presented in figure 5, a more accurate solution would be to determine the correction factor as a function of the distance between the CG and the volume centroid.

The empirical correlation factors were calculated for several Army Navy Spinner Rocket (ANSR)⁴⁶ configurations, shown in figure 22. Each of the three bodies had three CG locations, for a total of nine points. The determined correlation factors were plotted against the value $(X_{vc} - X_{cg})/D$ and the results were nearly linear in nature as shown in Figure 23. A linear curve fit was applied, resulting in equation 43.

$$K_E = -0.097 \frac{X_{vc} - X_{cg}}{D} + 0.4404 \quad (43)$$

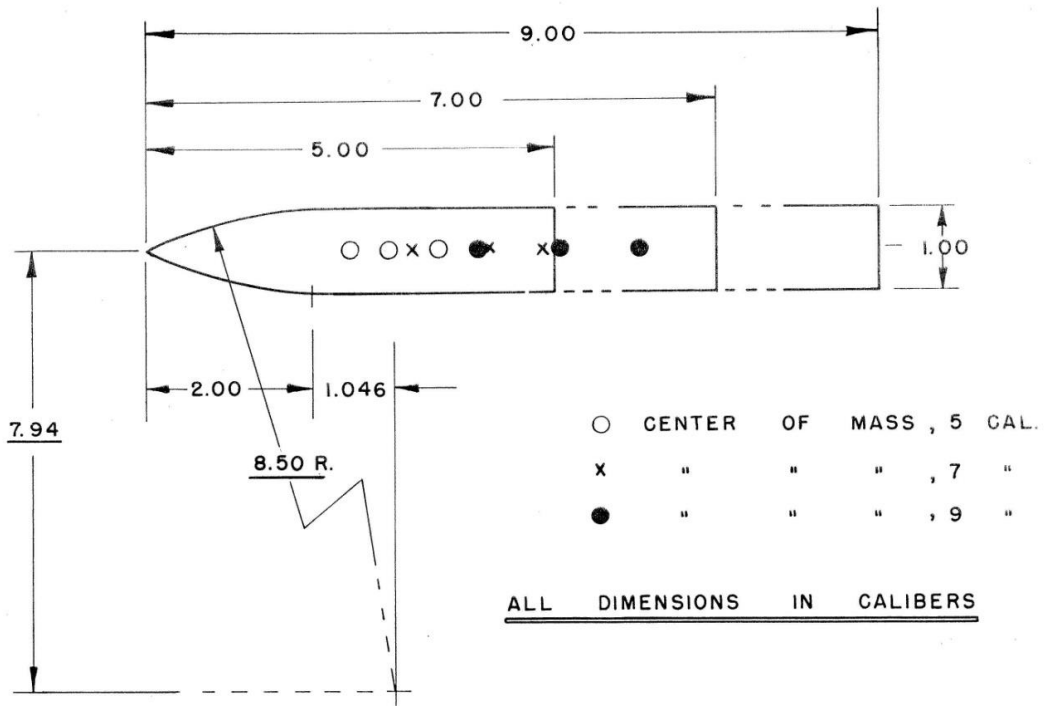


Figure 22. ANSR Configurations⁴⁶

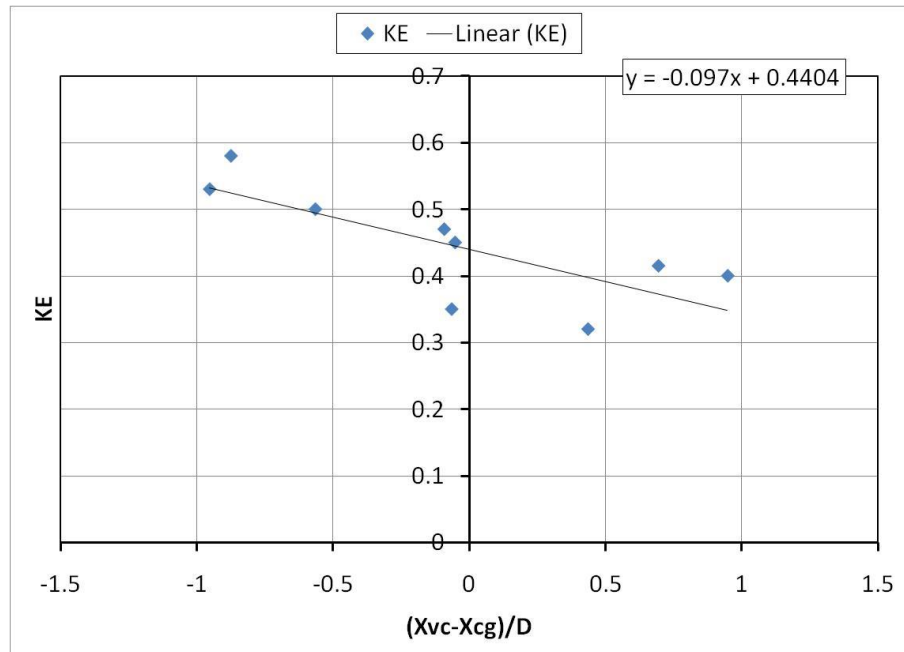


Figure 23. KE as a Function of Xcg Location

Unlike the Mach correlation factor, this empirical factor was developed with a very limited data set. As a result, this should not be taken as the final form of the equation. However, lack of experimental data makes it difficult to obtain more certain forms of the equation. Another point of interest in this development was the dependence of KE on the length of the body. As body length increased, there was less variation in KE as a function of $(X_{VC} - X_{CG})/D$. This trend is evident in Figure 24. The data points are identical to Figure 23 but they have been separated by body length. Over the CG ranges for the bodies, the KE values for the 5 caliber configuration varies by approximate 0.2 while the values for the 9 caliber configuration vary by approximately 0.13. This seems to indicate that as the body becomes sufficiently long, it is not necessary to present KE as a function of XCG location. Due to the lack of data, it is not possible to determine where this break point will occur. As a result, the two forms of KE presented in this section will be utilized in the following section. This will result in the equations 44 and 45 for $C_{M\dot{\theta}}$.

$$C_{m\dot{\theta}} = -2K_{ma}\cos\alpha \left(\frac{l}{d}\right)^2 \left(\sqrt{K_{ma}} - \frac{X_{cg}}{l}\right)^2 \quad (\text{for } KE = 0.5) \quad (44)$$

$$C_{m\dot{\theta}} = -4K_{ma}(-0.097\frac{X_{vc}-X_{cg}}{D} + 0.4404)\cos\alpha \left(\frac{l}{d}\right)^2 \left(\sqrt{K_{ma}} - \frac{X_{cg}}{l}\right)^2 \quad (45)$$

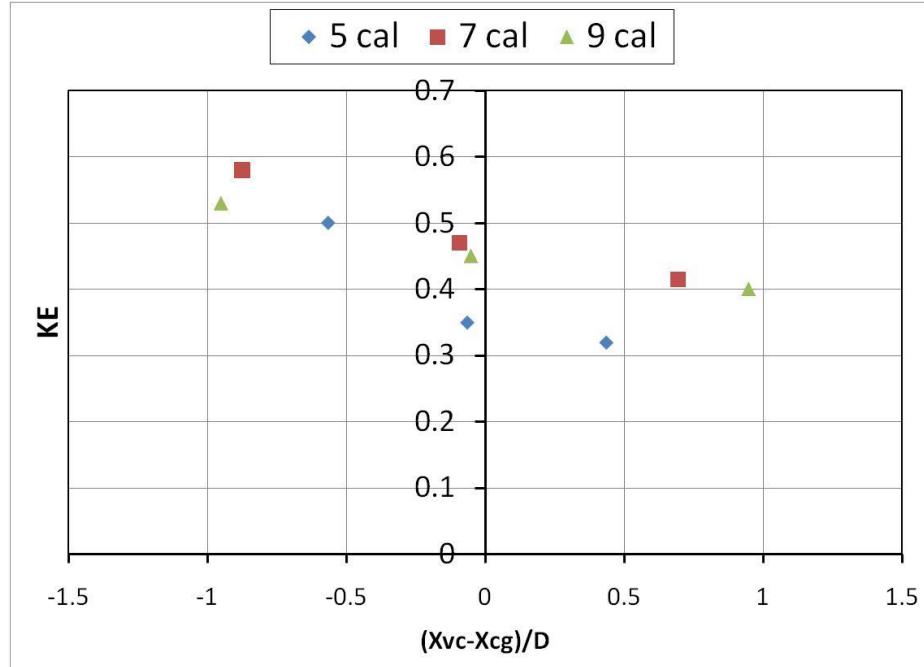


Figure 24. KE Variation with Body Length

Since $C_{N\alpha}$ was calculated from slopes at low angles of attack, the results are valid only at low angles of attack. However, future efforts will examine ways to obtain the high angle of attack pitch damping terms. Comparisons with experimental data are presented in the following section.

5.2 Evvard's Theory

Evvard's theory, as it is referred to in modern representations of the theory, is an extremely powerful, but often overlooked, means of calculating the loading on a supersonic lifting surface⁴⁷⁻⁵⁶. It is a purely theoretical approach based on the supersonic, linearized potential flow equations. In its original form, the theory is impractical for use in the calculation of damping derivatives for realistic configurations including wings and bodies. This is due to the fact that the theory does not account for the wing body junction. Although several efforts have been made to reduce Evvard's theory to simplified equations for standard wing shapes, this again limits the use for arbitrary configurations. This section details the updates and advancements made to Evvard's theory to develop and expand its

applicability to arbitrary wing body configurations while maintaining efficient calculations.

Evvard's theory makes use of the Mach lines that divide a thin supersonic wing into sections, as shown in figure 25. In each region, the velocity potential can be determined as a constant function of the x and y locations on the surface.

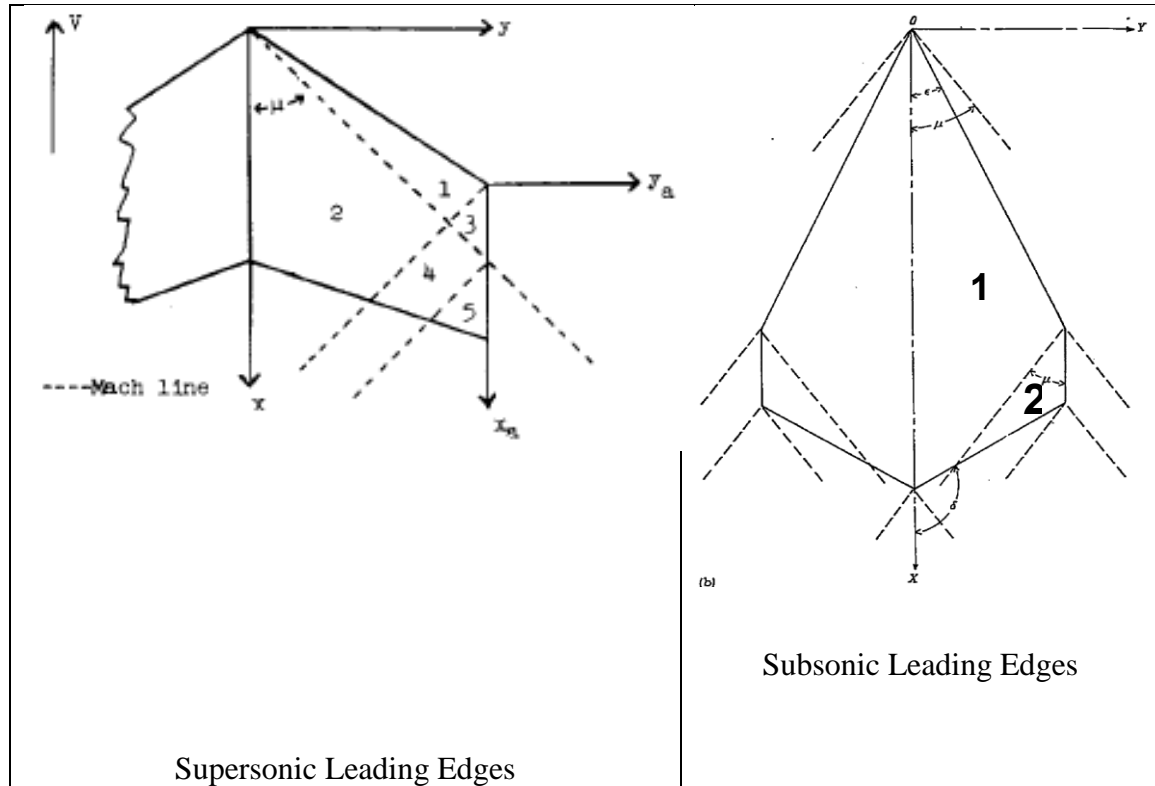


Figure 25. Mach Line Divisions

Evvard's theory represents a potential flow solution for a point source distribution over a thin, planar wing in supersonic flow. The initial method has been extended by several researchers to account for varying wing shapes and flow conditions⁴⁹⁻⁵⁸. These flow conditions include steady angle of attack, steady changes in angle of attack ($\dot{\alpha}$), steady pitching (q), and steady rolling (p). Many researchers have used Evvard's theory to develop exact equations for roll and pitch damping on various wing shapes. However, there are inherent difficulties with using the method in these formats. The most obvious

issue is that the equations are developed for very specific geometries thereby limiting their use for generic wing planform designs. Additionally, Evvard's theory is derived for a wing joined at the centerline. This makes it difficult, if not impossible, to use the exact equations for the practical problem of a wing in the presence of a body. This is due to a Mach line emanating from the wing body joint rather than the centerline of the wing alone system. Finally, visual observation shows that the equations are lengthy and cumbersome. Therefore, a more generic form of Evvard's equations where the aerodynamic coefficients are calculated from the pressure coefficient has been developed as a more practical and efficient use of the methodology.

In this theory, the wings are covered with a point source distribution⁵ that prevents flow from passing through the wing. From this source distribution, the velocity potential at any point on the wing can be determined. From this potential, it is then possible to calculate the differential pressure on the wing from equation 46^{53,54}.

$$\Delta C_p = \frac{4}{V_\infty} \frac{\partial \varphi}{\partial x} \quad (46)$$

The differential pressure represents the difference in loading between the upper and lower surfaces of the thin wing and is a function only of the single flow type that is being considered (i.e. p, q, α , etc). A separate ΔC_p can be determined for each type of motion a wing is undergoing at a given instant. Previous research^{53,54} has shown that the contribution from each type of motion can be summed to get the total loading on the fin. In other words, the pressure coefficient can be written as in equation 47.

$$\Delta C_p = \Delta C_p|_{\alpha} + \Delta C_p|_p + \Delta C_p|_q + \Delta C_p|_{\dot{\alpha}} + \dots \quad (47)$$

It is evident from this equation that this is a viable means for computing the damping derivatives that are of interest in this work. Since a given motion does not affect any other terms, it is possible to isolate the effect of the desired motion.

Because Evvard's theory is concerned with supersonic flow, only the portion of the wing in the upstream running Mach cone can affect any particular control point. Figure 26

illustrates the Mach cone emanating from a control point and the shaded region represents the area that can affect the loading at the control point. Points behind the Mach cone are contained in the zone of silence and therefore do not affect the loading at the control point.

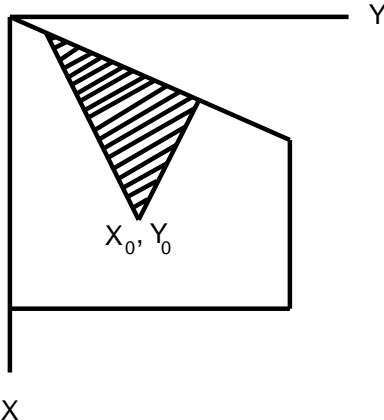


Figure 26. Schematic of Region of Influence for an Arbitrary Control Point⁵³

5.2.1 Roll Damping

In order to determine the roll damping coefficient using Evvard's theory, it is necessary to define the differential pressure coefficient due to a rolling motion. From this value, it is then possible to calculate the roll damping coefficient from the following equation.

$$C_{lp} = \frac{1}{sd(pd/2V)} \iint \Delta C_{p,p} y dx dy \quad (48)$$

Note that in equation 48, $\Delta C_{p,p}$ represents the differential pressure coefficient due only to the rolling motion. A closed form equation for each region of the wing as divided by the Mach lines has been developed by various researchers. The equations for the supersonic leading edge and subsonic leading edge divisions are shown in tables 5 and 6, respectively. These equations have been developed from the original theory into a formulation that is practical for an engineering level prediction.

Table 5. Differential Pressure Equations Due to Rolling Motion, Supersonic Leading Edge⁵³

Region	ΔC_p
1	$\frac{4pm^2x(\beta^2m^2v-1)}{V(\beta^2m^2-1)^{3/2}} \quad (49)$
2	$\frac{4pm^2x}{\pi V(\beta^2m^2-1)^{3/2}} \left[(1 + \beta mv) \cos^{-1} \frac{(1+\beta mv)}{\beta m(1+v)} - (1 - \beta mv) \cos^{-1} \frac{(1-\beta mv)}{\beta m(1-v)} \right] \quad (50)$
3	$\frac{4pm^2x(\beta^2m^2v-1)}{V(\beta^2m^2-1)^{3/2}} + \frac{4pm^2x(\beta mv-1)}{\pi V(\beta^2m^2-1)^{3/2}} \left\{ \left(mx_a - \beta my_a - \frac{b}{2}(1 - \beta mv) \right) \cos^{-1} \frac{mx_a-y_a(1-2\beta m)+b}{mx_a+y_a+b} - 2\beta m \sqrt{-y_a(\beta m - 1)(mx_a + \beta my_a + b)} \right\} \quad (51)$
4	$\frac{4pm^2x}{\pi V(\beta^2m^2-1)^{3/2}} \left[(1 + \beta mv) \cos^{-1} \frac{(1+\beta mv)}{\beta m(1+v)} - (1 - \beta mv) \cos^{-1} \frac{(1-\beta mv)}{\beta m(1-v)} \right] + \frac{4pm^2x(\beta mv-1)}{\pi V(\beta^2m^2-1)^{3/2}} \left\{ \left(mx_a - \beta my_a - \frac{b}{2}(1 - \beta mv) \right) \cos^{-1} \frac{-[mx_a+(2\beta m+1)]}{mx_a-y_a} - 2\beta m \sqrt{-my_a(x_a + \beta y_a + b)} \right\} \quad (52)$
5	$\frac{4pm^2x}{\pi V(\beta^2m^2-1)^{3/2}} \left\{ \left[mx_a + \beta^2m^2y_a + \frac{b}{2}(\beta^2m^2 + 1) \right] \cos^{-1} \frac{mx_a-y_a(1-2\beta m)+b}{mx_a+y_a+b} - 2\beta m \sqrt{-y_a(\beta m - 1)(mx_a + \beta my_a + b)} \right\} \quad (53)$

Table 6. Differential Pressure Equations Due to Rolling Motion, Subsonic Leading Edge⁵³

Region	ΔC_p
1	$\frac{2p\theta^2}{V} \left(\frac{xv}{\sqrt{1-v^2}} \right) \frac{2(1-m^2)}{(2-m^2)-m^2} \quad (54)$
2	$-\frac{8p}{V\pi} \left[\frac{\theta [3\theta x+y(1-2m)-\frac{b}{2}(1+m)] \sqrt{\frac{b}{2}-y}}{3(1+m)\sqrt{x+y}(1+m)} \right] \quad (55)$

Equations 49 through 55 neglect one important contribution to the wing loading – the body carryover load. Although the roll loading on the body itself is considered insignificant for the roll loads commonly experienced by missiles, the body still imparts a load to the wing that must be considered. The basic forms of Evvard's theory do not account for the presence of the body as they were developed for wings alone. However, other researchers have developed methods to handle the wing body carry-over by modifying the source distribution at the body. In particular, Tucker and Piland²⁸ have developed an alteration to the region 2 pressure loading when the wing is in the presence of the body. However, this distribution has not previously been used to approximate the roll damping derivatives in a practical manner. To apply their alteration the following equation is used for control points in region 2 in place of the equation 50.

$$\Delta C_p = \frac{4p}{\pi V} \left[\left(2 \frac{r_b}{h} - 1 \right) \frac{\sqrt{x^2 - \beta^2 y^2}}{\beta^2 - k^2} + \frac{\sqrt{x^2 - \beta^2 y^2}}{\beta^2 - k^2} + \frac{a}{\sqrt{\beta^2 - k^2}} \left[\cos^{-1} \frac{kx - \beta^2 y}{\beta(x - ky)} + \cos^{-1} \frac{kx + \beta^2 y}{\beta(x + ky)} \right] + \frac{\beta^2 y - kx}{(\beta^2 - k^2)^{3/2}} \cos^{-1} \frac{kx - \beta^2 y}{\beta(x - ky)} - \left(2 \frac{r_b}{h} - 1 \right) \frac{\beta^2 y + kx}{(\beta^2 - k^2)^{3/2}} \cos^{-1} \frac{kx + \beta^2 y}{\beta(x + ky)} \right] \quad (56)$$

$$k = \tan \Lambda \quad (57)$$

$$h = C_r \tan \mu + r_b \quad (58)$$

The value of h in the above equation is the distance from the body centerline to the point where the root chord Mach line crosses the trailing edge. Using this carryover estimation places another restriction on the use of Evvard's theory for roll damping. In this case, the root chord Mach line may not intersect the tip chord. It must cross the trailing edge at some point along the span. Although this carryover equation was developed for rectangular and triangular wings, there is no limitation for its use with arbitrary planforms provided this restriction is met. The results of this usage are shown in subsequent sections.

5.2.2 Pitch Damping Due to Pitch Rate

Two terms contribute to the overall pitch damping of a vehicle: the damping due to a pitch rate and the damping due to a rate of change in angle of attack. By altering the boundary conditions, Evvard's theory is capable of modeling both terms of the pitch damping coefficient. The equations presented are limited to fins with straight tips and Mach numbers that divide the wing into no more than 4 sections. Carryover loading from the body to the wing is not considered in these equations.

The pitch damping due to a pitch rate is defined equation 59.

$$C_{mq} = -\frac{1}{\frac{qc}{2v} S_c} \iint_S x \Delta C_p dx dy \quad (59)$$

As with the roll damping coefficient, Evvard's theory defines the change in pressure coefficient due to the pitch rate – not the actual pitch damping term. The actual value of ΔC_p varies depending on the location of the wing. Table 7 defines the values of ΔC_p based on the region of the wing for a supersonic leading edge. Subsonic leading edges are not considered for the pitch damping as no experimental data exists to verify the results. Additionally, alternate computational approaches are not of sufficient accuracy to verify a new method.

Table 7. Pressure Coefficient Due to a Pitching Rate⁵⁷

Region	ΔC_p
1	$\frac{2q}{V(\beta^2 m^2 - 1)^{3/2}} [2mx(\beta^2 m^2 - 2) + 2y] \quad (60)$
2	$\begin{aligned} & \frac{4q}{\pi V} \left\{ \frac{2m\sqrt{x^2 - \beta^2 y^2}}{\beta^2 m^2 - 1} + \frac{2mx(\beta^2 m^2 - 2) - 2y}{2(\beta^2 m^2 - 1)^{3/2}} \cos^{-1} \frac{x + \beta^2 my}{\beta mx + \beta y} + \right. \\ & \left. \frac{2mx(\beta^2 m^2 - 2) + 2y}{2(\beta^2 m^2 - 1)^{3/2}} \cos^{-1} \frac{x - \beta^2 my}{\beta mx - \beta y} \right\} \quad (61) \end{aligned}$
3	$\begin{aligned} & \frac{4q}{\pi V} \left[\frac{2mx_a(\beta^2 m^2 - 2) + 2y_a + b(\beta^2 m^2 - 1)}{2(\beta^2 m^2 - 1)^{3/2}} \cos^{-1} \frac{mx_a + (2\beta m + 1)y_a}{mx_a - y_a} - \right. \\ & \left. \frac{2(1 + \beta m - \beta^2 m^2)}{\beta^2 m^2 - 1} \sqrt{\frac{-my_a(x_a + \beta y_a)}{\beta m - 1}} \right] \quad (62) \end{aligned}$
4	$\begin{aligned} & \frac{2q}{2V} \left\{ \frac{2mx_a(\beta^2 m^2 - 2) + 2y_a + b(\beta^2 m^2 - 1)}{2(\beta^2 m^2 - 1)^{3/2}} \left[\cos^{-1} \frac{mx_a + (2\beta m + 1)y_a}{mx_a - y_a} - \right. \right. \\ & \left. \left. \cos^{-1} \frac{-mx_a + \beta^2 m^2 y_a + \frac{b}{2}(\beta^2 m^2 - 1)}{\beta m(mx_a - y_a)} \right] - \frac{2(1 + \beta m - \beta^2 m^2)}{\beta^2 m^2 - 1} \sqrt{\frac{-my_a(x_a + \beta y_a)}{\beta m - 1}} + \right. \\ & \left. \frac{2\sqrt{(mx_a + \frac{b}{2})^2 - \beta^2 m^2(y_a + \frac{b}{2})^2}}{\beta^2 m^2 - 1} + \right. \\ & \left. \left. \frac{2mx_a(\beta^2 m^2 - 2) - 2y_a + b(\beta^2 m^2 - 3)}{2(\beta^2 m^2 - 1)^{3/2}} \cos^{-1} \frac{mx_a + \beta^2 m^2 y_a + \frac{b}{2}(\beta m + 1)}{\beta m(mx_a + y_a + b)} \right\} \quad (63) \right]$

5.2.3 Pitch Damping Due to Change in Angle of Attack

The pitch damping due to the rate of change in angle of attack is defined as follows in equation 64.

$$C_{m\dot{\alpha}} = -\frac{1}{\frac{\dot{\alpha}c}{2v} S_c} \iint_S x \Delta C_p dx dy \quad (64)$$

The change in pressure coefficient due to a rate of change in angle of attack is defined as follows in table 8. Again, these equations have been modified from the original in order to allow practical application of the theory.

Table 8. Pressure Coefficient Due to a Rate of Change in Angle of Attack⁵⁸

Region	ΔC_p
1	$-\frac{4\dot{\alpha}(mx-y)(m^2+1)}{V(\beta^2m^2-1)^{3/2}} \quad (65)$
2	$\frac{4\dot{\alpha}}{V\beta^2\pi(\beta^2m^2-1)^{3/2}} \left\{ 2M^2m\sqrt{(x^2 - \beta^2y^2)(\beta^2m^2 - 1)} - \beta^2(m^2 + 1) \left[(mx + 1)\cos^{-1}\frac{x+\beta^2my}{\beta(mx+y)} + (mx - y)\cos^{-1}\frac{x-\beta^2my}{\beta(mx-y)} \right] \right\} \quad (66)$
3	$\frac{4\dot{\alpha}}{V\beta^2\pi(\beta^2m^2-1)^{3/2}} \left\{ [\beta(\beta^2m^2 - \beta m - 1) - m]\sqrt{(b - 2y)(\beta m + 1)[2m(x + \beta y) - b(\beta m + 1)]} - \beta(mx - y)(m^2 + 1)\cos^{-1}\frac{mx-b(\beta m+1)+y(2\beta m+1)}{mx-y} \right\} \quad (67)$
4	$\Sigma(region\ 2 + region\ 3 - region\ 1) \quad (68)$

As noted in the previous section, subsonic leading edges are again not examined. In addition to the lack of comparative data, the sensitivity analysis presented in previous sections indicates a lack of relevancy for the majority of applications. Instead, these equations are presented for reference.

5.2.4 Practical Application of Evvard's Theory

The ability to use Evvard's theory on arbitrary wing shapes for body wing configurations is the crux of the work done under this effort. Direct application of Evvard's theory requires that the wings are separate panels joined at the root chord^{47,48}. The resulting Mach lines will originate from the apex of the wing junction. However, for most missile and aircraft configurations, the wings are not joined at the centerline and Mach lines originate from the wing body junction. This means that the wing must be extended into the body as shown in Figure 27^{53,54}. Points that are contained within the body diameter are given a pressure loading of zero so that they do not affect the overall loading the fins. However, the Mach lines will emanate from this joint at the center line of the body. As a result, for certain configurations, the discrepancy in the theoretical versus actual Mach lines

may significantly alter the loading. This discrepancy may be alleviated if the wing is extended into the body but the Mach lines are shifted to the wing body junction. An example is shown in Figure 28 for the basic finner wing. This essentially treats the wing itself as a single panel, but utilizes the coordinate system with the origin along the body centerline. This distinction is important for the determination of the proper value of the y coordinate. In particular, the roll loading varies with distance from the roll axis, in this case the body centerline, the y coordinates on the wing must originate from that point.

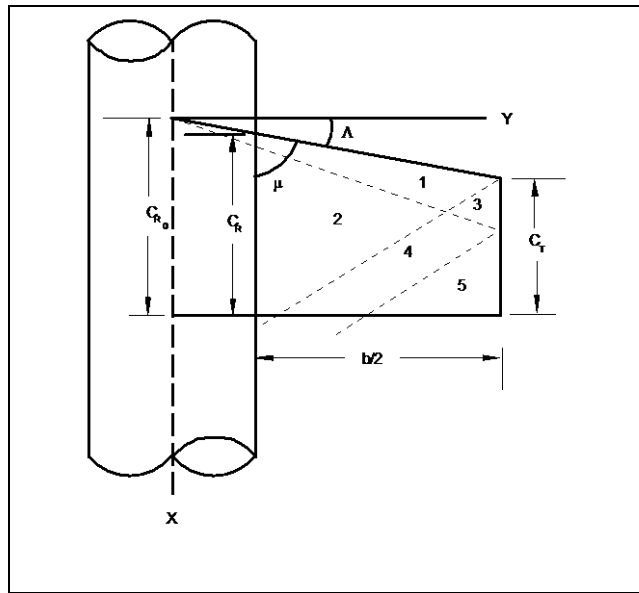


Figure 27. Fin Extension into the Body

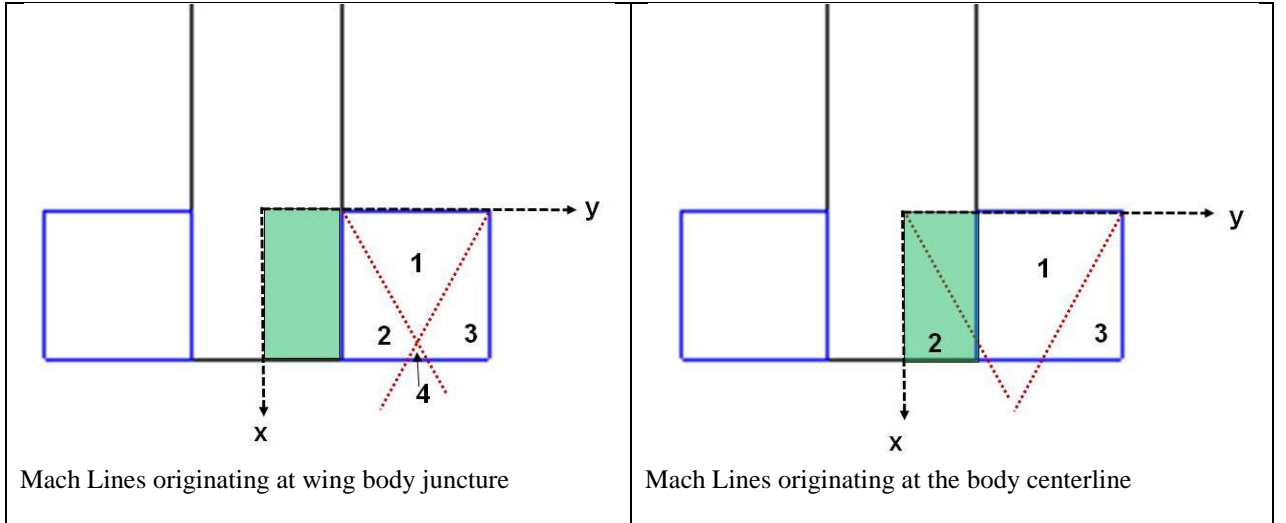


Figure 28. Mach Line Orientations

To apply Evvard's theory, a wing semi-span is divided into discrete panels with a control point located in each panel. The region in which a control point resides must be determined so that the proper pressure loading equation is utilized. This is done by defining the following variables, with y originating at the body centerline. Equations 69-71 define the Mach line locations at each chordwise (x) location on the fin.

$$x_1 = (y - r_b)\beta \quad (69)$$

$$x_2 = \tan \Lambda + \beta(1 - y) \quad (70)$$

$$x_3 = \beta(2 - y - r_b) \quad (71)$$

Next, equations 72-76 are used to determine which region a control point is in based on the x location of the control point. This setup is shown graphically in Fig. 29⁵⁹.

$$\text{Region 1: } x < x_1 \text{ and } x < x_2 \quad (72)$$

$$\text{Region 2: } x > x_1 \text{ and } x < x_2 \quad (73)$$

$$\text{Region 3: } x > x_2 \text{ and } x < x_1 \quad (74)$$

$$\text{Region 4: } x > x_1 \text{ and } x > x_2 \text{ and } x < x_3 \quad (75)$$

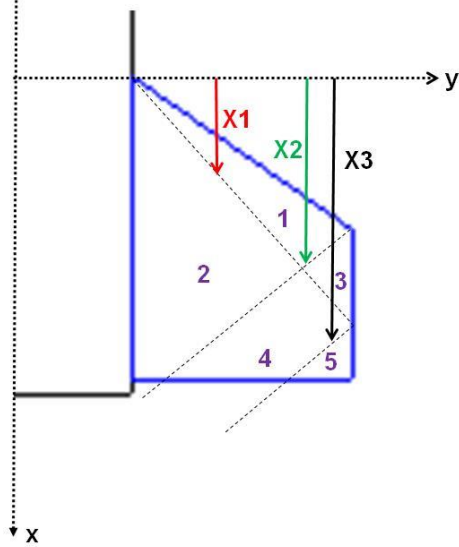


Figure 29. Control Point Determination

With proper region determined, the value of ΔC_p is calculated using the equations in Table 5. The values of ΔC_p are summed over the entire wing and the process is repeated for all wing in a given fin set. The value of roll damping is then calculated from the following equation.

$$C_{lp} = \frac{Vb}{4p} \sum_1^{n_{fins}} \sum \frac{\Delta C_p * da * y}{sref * d} \quad (77)$$

In the above equation, da refers to the incremental area of the panel in which a control point is located. It should be noted that the Evvard equations derive ΔC_p and thus C_{lp} as a function of the wing span. This effort converts the value of C_{lp} to be normalized by the reference length as is common in missile configurations.

5.3 Angle of Attack Effects

The methods developed in this effort has been limited strictly to zero angle of attack. In practicality, the results presented would be valid at low angles of attack in order to adhere to the principles of potential flow. It is noted that the equations presented are not

functions of angle of attack due to this linear assumption. Additionally, the driving principle behind Evvard's theory is the fact that angle of attack effects can be separated from the effects induced by motion, as shown in equation 47. As a result, according to Evvard's theory, the damping terms are not functions of angle of attack. For the purpose of most missile flight, the high angles of attack presented are not necessary and the results may be of questionable importance.

This fact however, does not mean that damping derivatives are not functions of angle of attack. There has been recent work done in the area of high angle attack and non-linear damping derivatives presented by Moore^{60,61}. Moore used two approaches to improve the non-linear, or high angle of attack, methods for both pitch and roll damping in his Aeroprediction code. The first was to improve the linear zero angle of attack predictions of both static and dynamic aerodynamics already inherent in the code by using new experimental data to improve the empirical methods. The second was to develop a correlation between the zero angle of attack damping derivatives and limited high angle of attack data. These methods are strictly empirical and have not been thoroughly validated as noted by Moore himself. Figures 30 and 31 illustrate the work of Moore and the limited datasets available for correlation.

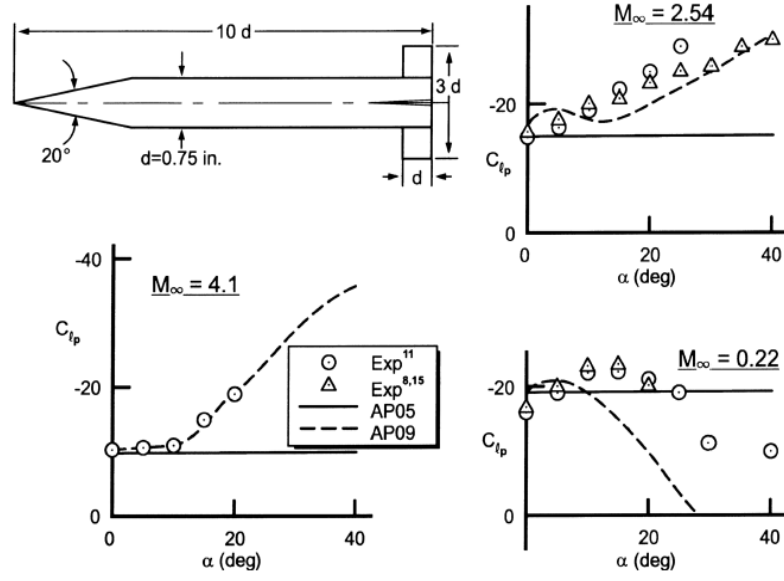


Figure 30. Updated Rolling Damping Calculations by Moore⁶⁰

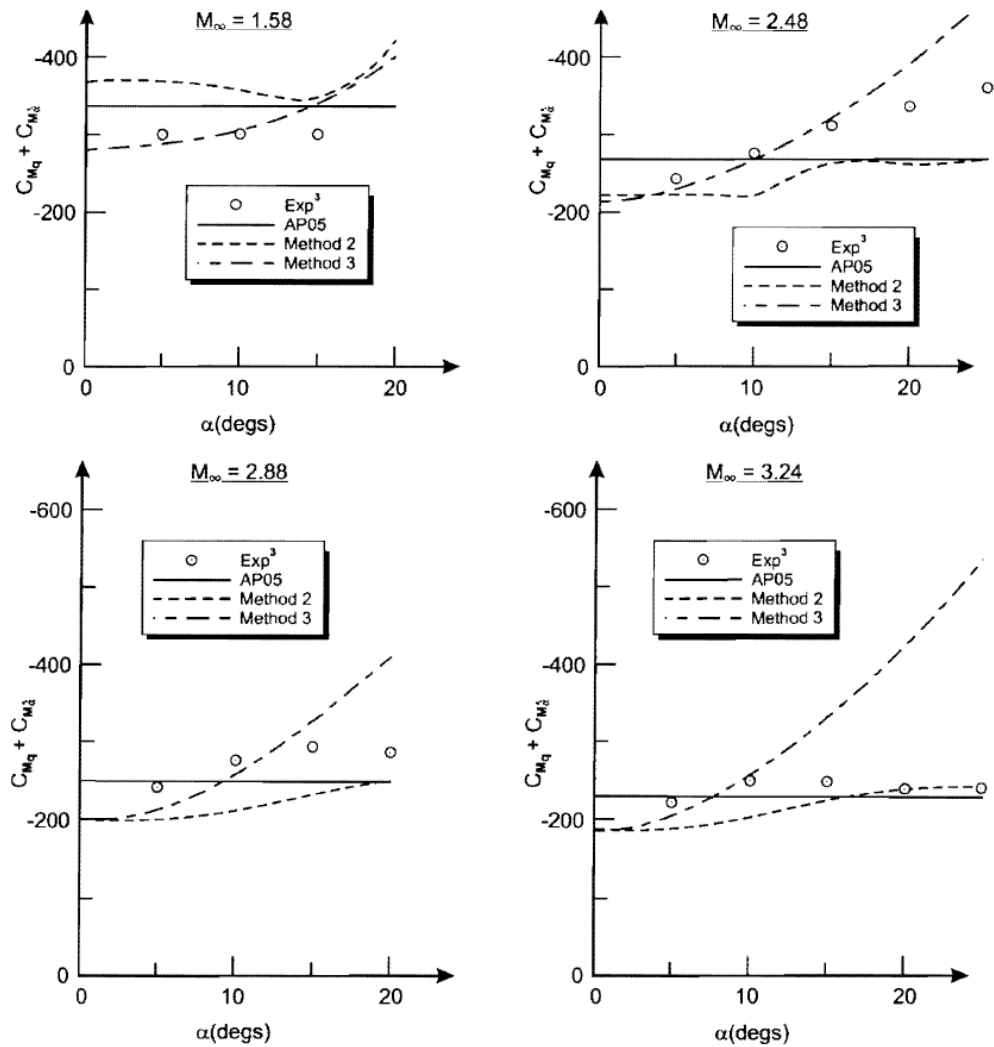


Figure 31. Updated Pitch Damping Calculations by Moore⁶¹

6 Verification and Discussion

Previous sections have presented standard and newly developed methodologies for calculating the supersonic pitch and roll damping derivatives for arbitrary body, wing, and wing and body combinations. The follow section compares the results from these methodologies with experimental data and/or other available approaches. Available supersonic pitch damping data is extremely limited. The basic finner and modified basic finner encompass most of the available data; however, the data is at angles of attack and Mach numbers beyond the scope of this effort.

6.1 Body Alone Verification

The five caliber ANSR consists of a two caliber secant ogive with a 3 caliber cylindrical body. This is clearly not a slender body, however, it was used as a test case since there is a limited amount of data available. The results are shown in Figures 32 and 33. Experimental and CFD results were obtained from Park⁶² for Mach numbers 1.8 and 2.5 at three discrete moment reference point locations. The ESDU results were obtained directly from the reference⁴⁵ for this configuration though the moment reference points are slightly different. The ESDU results provide the best match to the CFD and experimental results. This is to be expected as this modification of slender body theory was developed for bodies of this size. Basic Slender body theory provides the worst approximation, while Datcom⁶ and the current effort improve the basic theory. The value of KE greatly impacts the current method though one is not necessarily an improvement over the other. Datcom typically provides a better estimate than either of the KE approaches. This is likely due to the value of KM being developed for longer bodies. If shorter configurations were considered, the current approach(es) may show better accuracy. The lack of verifiable data for shorter configurations precluded such analysis.

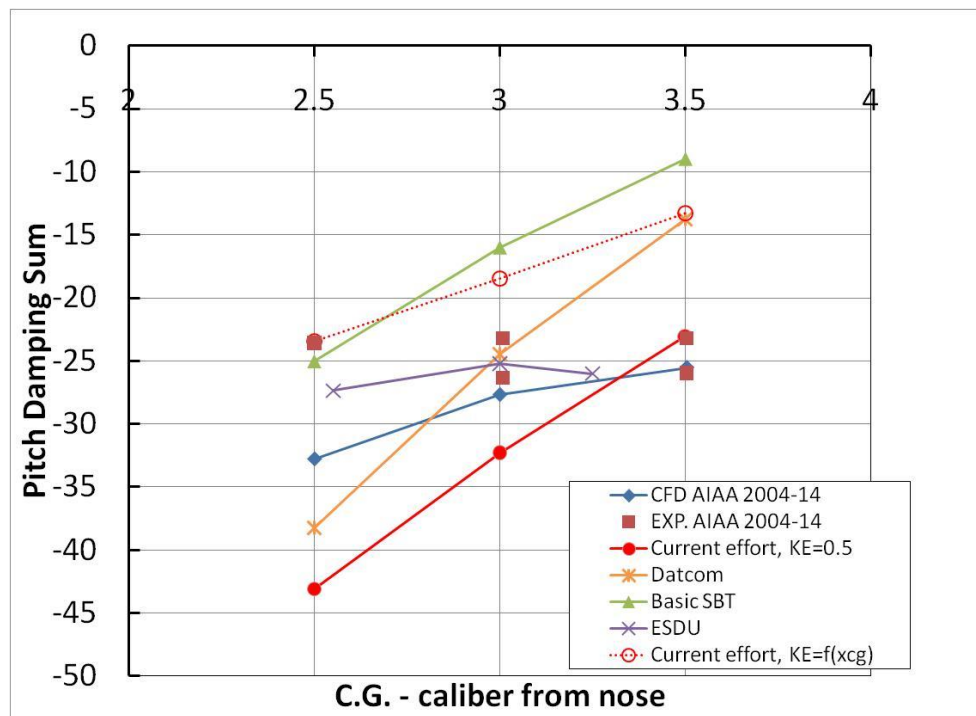


Figure 32. 5 Caliber ANSR Results, Mach 1.8

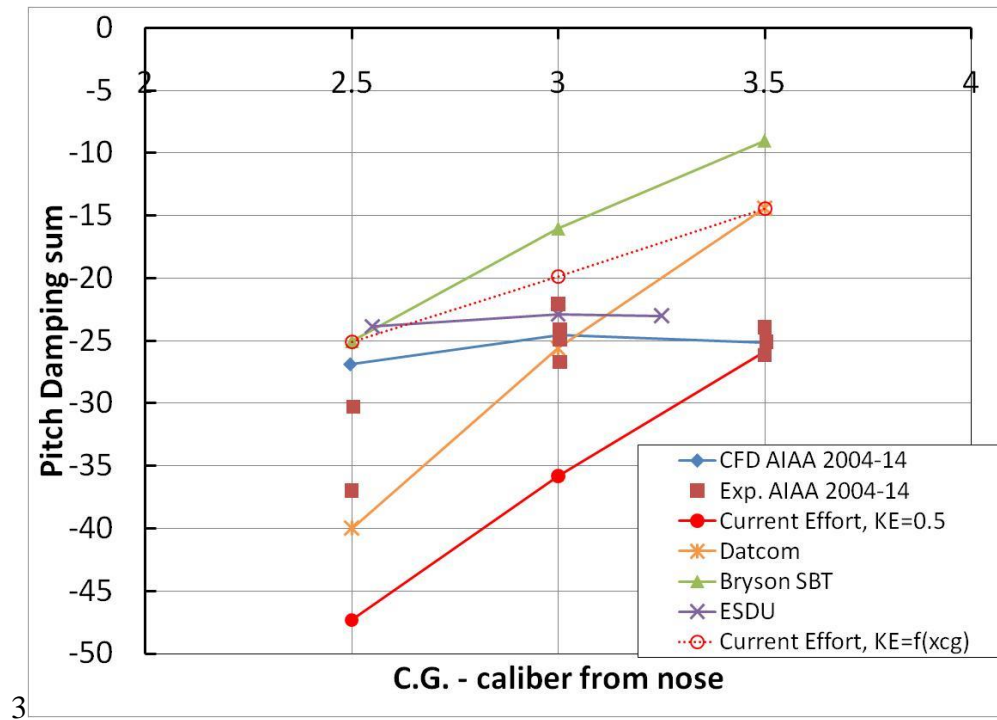


Figure 33. 5 Caliber ANSR Results, Mach 2.5

The 7 caliber ANSR configuration is a 2 caliber secant ogive nose and a 5 caliber body. Though still not a true slender body, it is a better representation than the previous configuration. Experimental and CFD data was obtained from DeSpirito⁶³. Data was given as a function of Mach number for three different moment reference point locations: 3.25 cal, 4.036 cal, and 4.818 cal aft of the nose. Comparisons are presented in figures 34-36. ESDU results are not presented for the 3.25 caliber CG location as the F1 correction factor was not defined by the reference. Additionally, Datcom values of $C_{N\alpha}$ are used for the ESDU computation at the other CG locations as it was not possible to obtain values from the reference.

It is clear from these results that the limitation of basic slender body theory lies in its Mach independency. All of the modified slender body methods provide some degree of correction for Mach number variation. The accuracy of each method is dependent on CG location and Mach number. Unlike with the 5 caliber configuration, the ESDU approach is the worst approximation. This is expected given the empirical correlations were developed for shorter bodies. Datcom is typically within 20 percent of the experimental values, although that accuracy degrades with rearward shifts in CG location. Regardless of KE value, the accuracy of the current approach improves with rearward shift in the CG location. At the center CG location, predictions are within 5 percent of the CFD data when KE values tied to the CG location is used. Although there are some points that are slightly higher, using a KE value tied to the CG location typically produces results within 10 percent of the experimental values while the constant KE value is typically within 15 to 20 percent of experimental values.

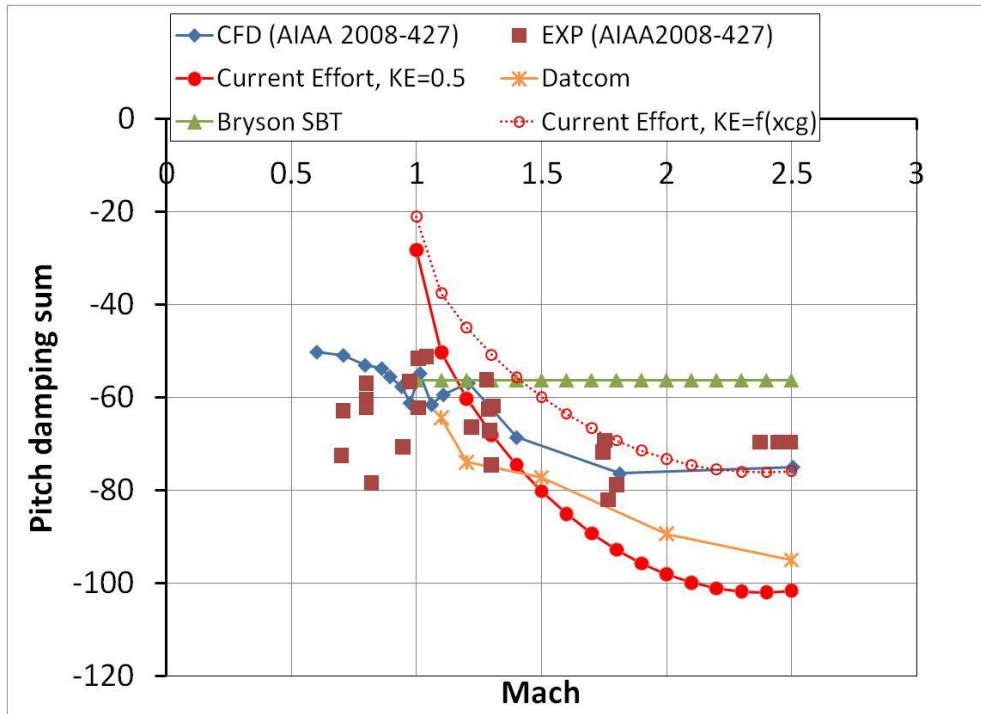


Figure 34. 7 Caliber ANSR Results, XCG=3.25 Calibers Aft of Nose

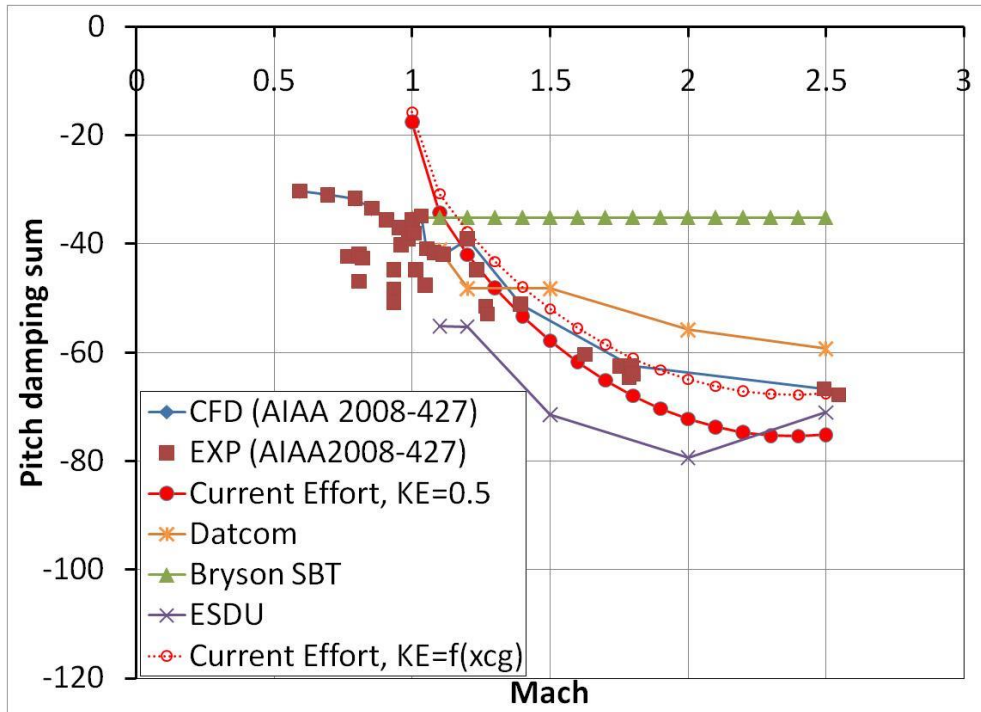


Figure 35. 7 Caliber ANSR results, XCG=4.036 Calibers Aft of Nose

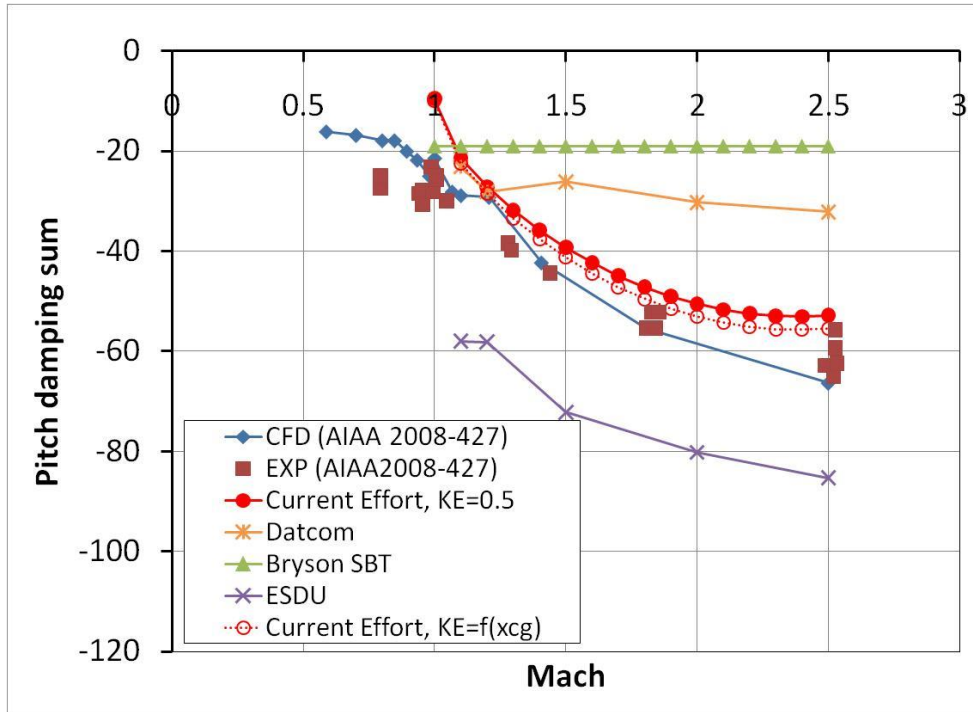


Figure 36. 7 caliber ANSR Results, XCG=4.818 Calibers Aft of Nose

The 9 caliber ANSR is a 2 caliber secant ogive with 7 caliber centerbody and is most typical of a slender body configuration. Results are presented in figures 37 and 38 Again, experimental data was obtained from Park¹⁹. ESDU results are not presented for this configuration as it is outside the range of the empirical correlations for that theory. For this configuration, the methods developed in this paper provide a significant improvement over both basic slender body theory and Missile Datcom. Regardless of KE value, the current effort is within 10 percent of the experimental results. Using a value of KE that varies with CG location provides an even better estimate. The fact the current method works best for this configuration is not a surprise as it is closest to the body lengths used to develop Km.

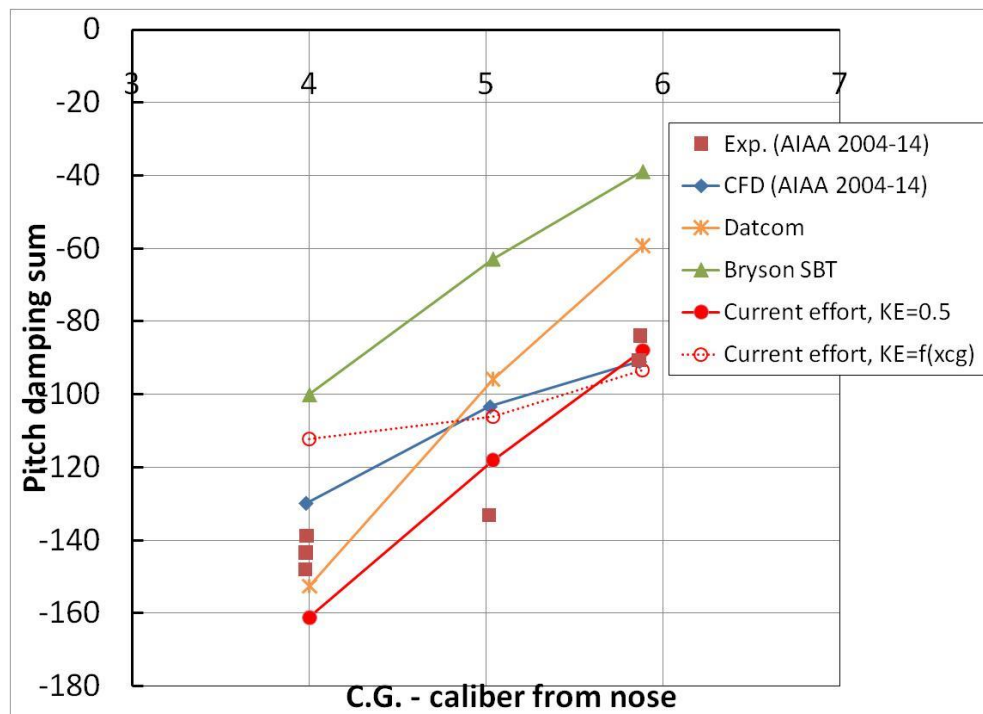


Figure 37.9 Caliber ANSR Results, Mach 1.8

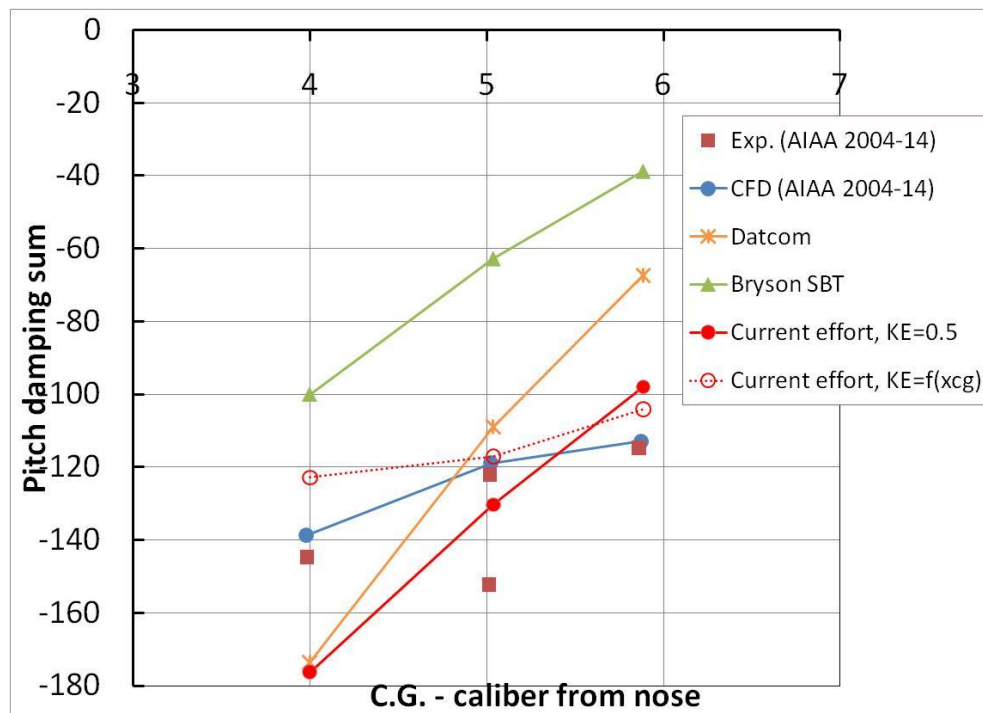


Figure 38.9 Caliber ANSR Results, Mach 2.5

6.2 Complete Configuration Verification

As with the individual component analysis, there is a limited amount of test data available for comparison. It should be noted that the majority of the data is derived from historical wind tunnel data for which statistical analysis is not available or possible. Therefore, comparisons are presented only for roll damping as this is the most widely verified data set.

Basic Finner is a standard research configuration for which extensive test data exists^{34-39,64,65}. This makes it an ideal configuration for evaluating roll damping methodologies. For the comparisons shown in this section, experimental results from references 68 and 69 were used. Reference 64 provided roll damping uncertainties of $\pm 2.5\text{-}\pm 3.5$ percent for the data range considered and Mach number accuracy of ± 1 percent. Data uncertainty was not available for reference 65. The slender body theory and Eastman³⁰ equations presented in Section 3 were used to obtain their representative curves. In order to calculate the value of $C_{l\delta}$ needed for the Eastman calculation, the 2011 version of Missile Datcom⁶ was used. A 5 degree roll deflection was applied to each fin and the value of $C_{l\delta}$ was obtained using the following equation.

$$C_{l\delta} = \frac{C_{l\delta=5} - C_{l\delta=0}}{\delta} \quad (105)$$

The value of the y centroid of the fin was found from a Missilelab⁶⁶ analysis of the fin geometry. Since a plain hexagonal cross section was used to model the fin, it is possible that the y centroid is slightly off and may skew the results slightly.

It is noted in the comparisons that there is a slight scatter in the experimental data. Still it is possible to see a general trend of decreasing roll damping with increasing Mach number. With the exception of slender body theory, all of the methods presented in Figure 39 show this same trend. Slender body theory is by definition invariant with Mach number, but seems to provide the best match near Mach 2.5. Eastman's method follows the trend quite well, though the roll damping is under predicted by approximately 10-15 percent

across the Mach range. Given that basic finner is one of the test cases for Eastman's theory, the accuracy is not surprising. The Evvard methodology provides a slightly better approximation of the roll damping. The values are slightly under predicted if body upwash is excluded and near exact to slightly over predicted if the upwash is included. Since the effect of the upwash is to increase the pressure loading near the fin body junction, this increase in damping is to be expected. Additionally, as Mach number increases, the effect of adding the upwash decreases. This is due to the decrease in the Mach angle and therefore the decrease in the region over which the upwash is acting.

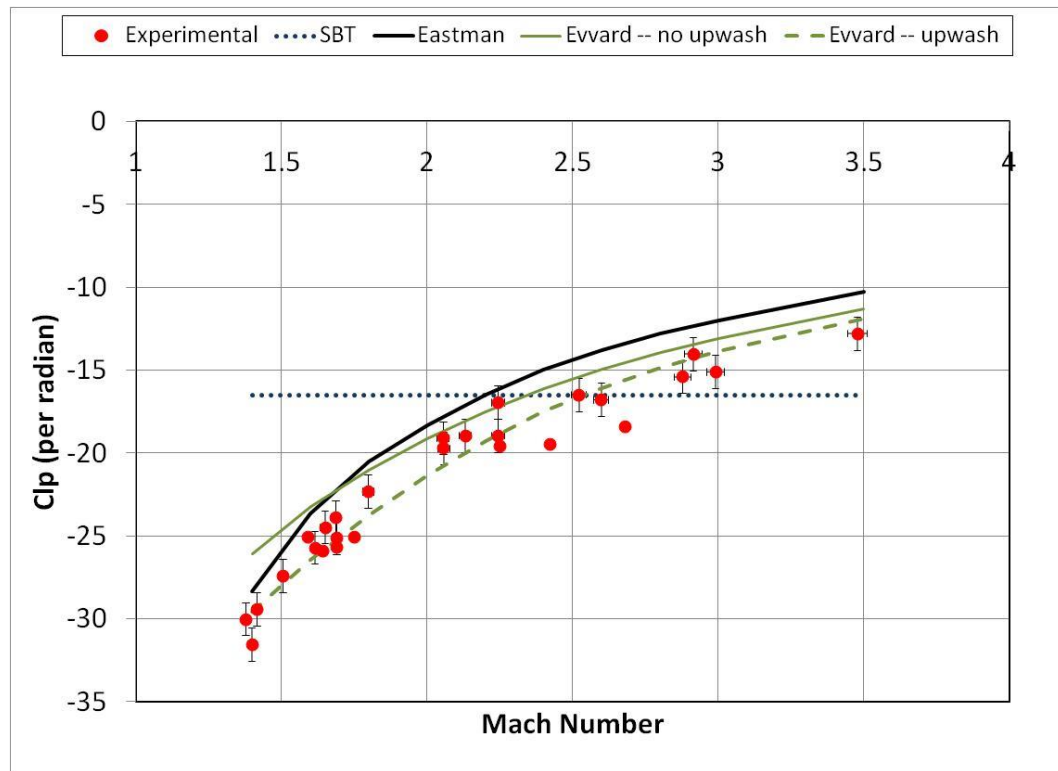


Figure 39. Results for Basic Finner Roll Damping

The modified basic finner is another configuration for which a significant amount of damping data exists^{38,65}. The body of the modified finner configuration is identical to the basic finner; however the fin has been altered. The fin area of the modified finner is

roughly half that of the basic finner. The dimensions of the fin are shown in Fig. 40. Experimental data for the modified finner were obtained from reference 38 and 65. As with the basic finner data from this reference, no indication of the data uncertainty was provided.

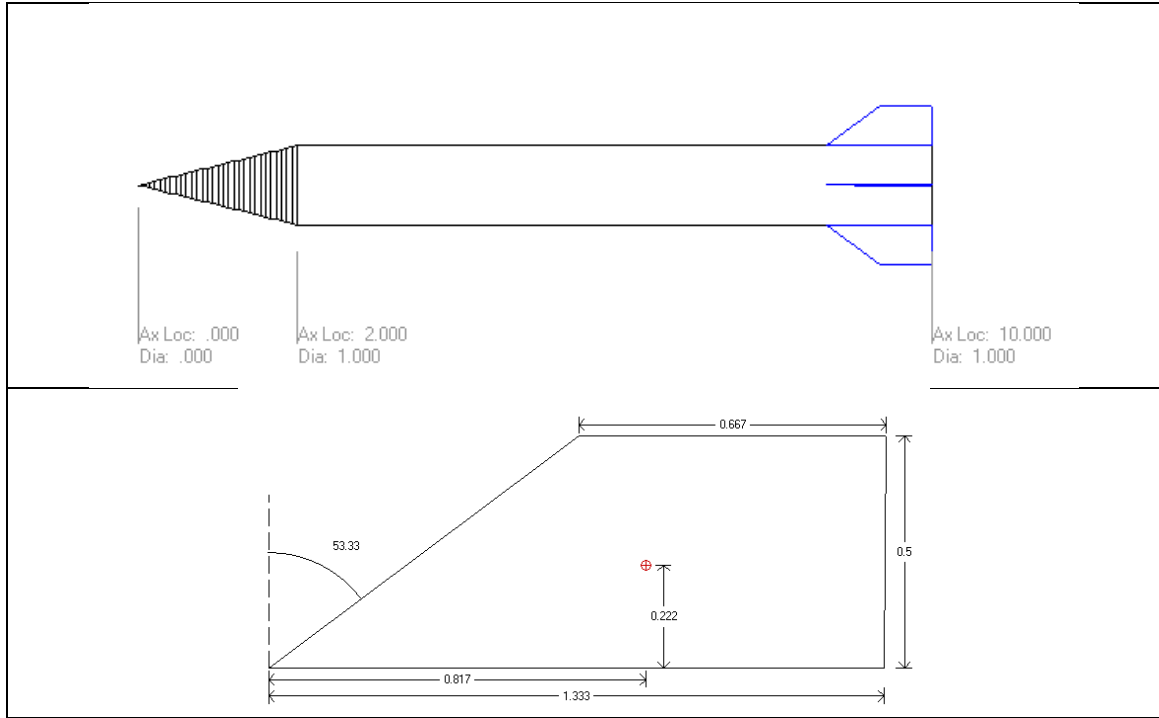


Figure 40. Modified Finner Geometry

Results for the modified basic finner are shown in Figure 41. As seen with the basic finner configuration, slender body theory is the least accurate method for obtaining the roll damping. In this instance, Eastman's method tends to over predict the roll damping across the range evaluated in this effort. As this configuration was also one of Eastman's test cases, this difference could be caused by inaccuracies in the value of $C_{l\delta}$ or y_{cent} , which were again obtained via Missile Datcom⁶ and MissileLab⁶⁶.

Evvard's analysis provides the most accurate approximation of the roll damping given the methods under consideration. As Mach number increases, Evvard's theory tends

to slightly over predict the roll damping values. This is slightly different than the trends seen for basic finner where Evvard's theory under predicted the damping if upwash was excluded.

It is noted that body upwash is not considered for this particular configuration. Recalling that the root leading edge Mach line may not intersect the wing, the body upwash calculations are not valid until the Mach number exceeds 2.8. This value is well beyond the range of available experimental data for this configuration. Even at this Mach number, the root Mach line will intersect the fin very close to the tip. This trend is true of most low aspect ratio configurations. As such, the upwash characteristics need to be considered for fins of this nature. Even without the upwash, Evvard's theory provides a more accurate approximation to the damping than the other easily available methods.

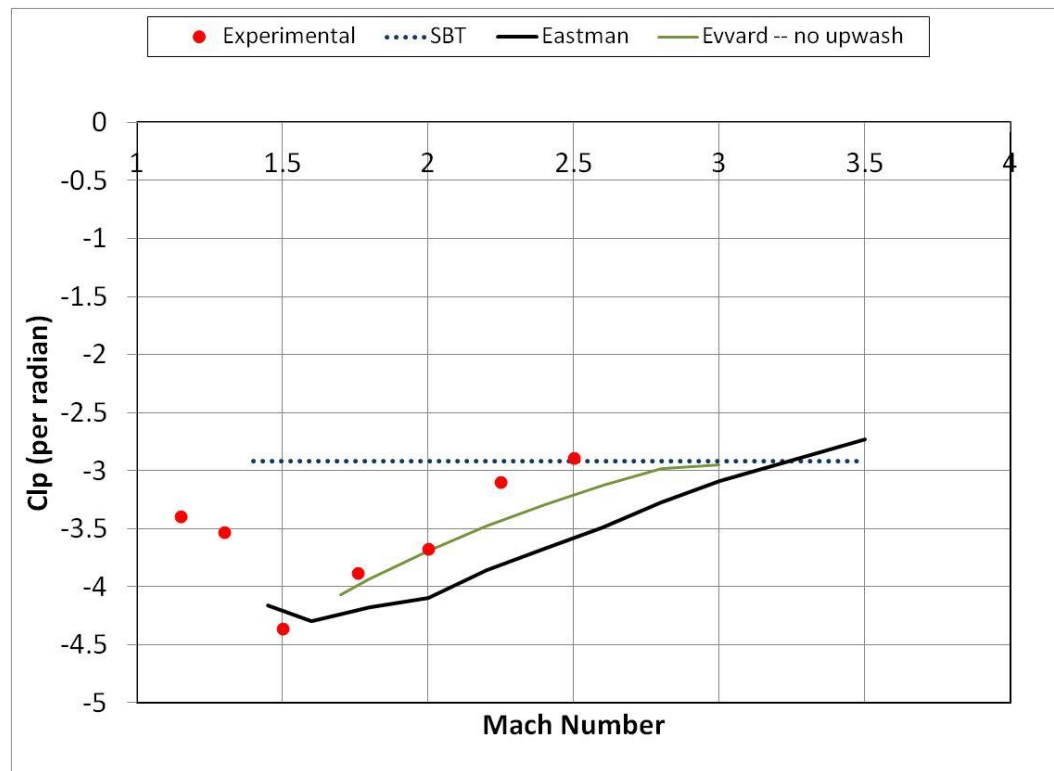


Figure 41. Modified Finner Clp

7 Conclusions and Recommendations

The work presented in this dissertation provides the engineer with a new and unique approach to calculating the damping derivatives of supersonic configurations with a basis in potential flow aerodynamics. New semi-empirical methods have been added to expand classical slender body theory to a wider subset of body alone configurations. The use of Evvard's theory to calculate the lifting surface terms represent a novel and easily accessible means of determine the derivatives for arbitrary configurations. Applying a configuration synthesis approach further expands the usefulness to the community at large. The results are on par with more computationally expensive CFD results. Additionally, the results are an improvement over the standard semi-empirical results produced in typical engineering level design tools. The result is a higher degree of accuracy in damping derivative calculation at less expense. This makes the methods developed a desirable approach for preliminary design work as well as production level work for systems possessing low sensitivity.

The purpose of this work is to assess the overall usage, evaluation, and understanding of damping derivatives with a focus on accuracy needs and computational efficiency. Although much progress has been made with regard to static aerodynamics with both accuracy and efficiency of calculation, dynamic stability has lagged behind due to the complex nature of the aerodynamics and the variable sensitivity of the system to variations in the terms. As a result, a methodology was developed to assess the importance of the derivatives for a given configuration and new methods were developed for computation of the body and fin derivative separately in order to provide a configuration synthesis computation. A generic missile configuration, the basic finner, was used as the vehicle for many of the calculations and comparisons in this effort. Although more complex vehicles are desired, the lack of investments in dynamic stability calculations has led to a lack of available test data to compare existing and new approaches. There are no limitations to

the methods that would preclude their use on more complex systems, assuming flow attachment and Mach number constraints are met.

As part of this effort, a sensitivity analysis was conducted to give a surface level understanding of the importance of damping derivatives. This was by no means an exhaustive evaluation of the overall sensitivity. Such an analysis would be extremely specific to a given vehicle and flight regime. It is recommended, however, that more attention be provided to the sensitivity of a system to various aerodynamic terms. Such an approach would lead to more efficient allocation of computational and experimental resources in a budget constrained environment. A complete design of experiments approach while developing a new configuration would lend significant insight to the importance of such terms and the investment that should be given toward their development.

The methodologies examined developed under this effort provide a means for the calculation of pitch and roll damping for supersonic Mach numbers. Results and trends compare favorably with existing, limited experimental data. The methodologies presented offer improvements in both accuracy and ease of use over existing empirical means for calculating damping derivatives. However, the methodologies presented in this study have limitations that should be expanded under future efforts. In particular, all of the methods are limited to zero degrees angle of attack. This was done due to the complexity of the flowfields and angle of attack, a lack of available experimental data, and an uncertainty in the importance of the damping derivatives at moderate to high angles of attack. Additionally, vortex lattice approaches were considered as an alternate approach for these calculations. Due to the nature of the problem and the complexity of configurations, the method was abandoned for this effort. However, this does not preclude the use of vortex lattice approached for the calculation of damping derivatives. This is yet another area where future work may benefit the community. Also not addressed under this effort are the implications and analysis of transonic flight. As this is often a region of interest for many missile configurations, it should be considered under future efforts.

Another limitation of this effort is a lack of experimental data. Reliable data for varied conditions exists only for a limited subset of configurations. Although it is unlikely

that wind tunnel resources will be expended to increase the available data set, CFD is rapidly becoming a reliable means to obtain dynamic aerodynamic terms. As a result, it may be used as a means to prove the accuracy of the faster, lower order potential flow methodologies presented under this effort. Additionally, as resources improve, it will become a necessary method for dynamic stability and control approaches, particularly for systems that require highly accurate calculations of these terms.

References

1. Shevell, R.S. *Fundamentals of Flight*, Prentice Hall, New Jersey, 1989.
2. Etkin, B., Reid, L.D., *Dynamics of Flight: Stability and Control*, John Wiley & Sons, Inc., New York, 1996
3. DeSpirito, J., Silton, S. I., Weinacht, P., "Navier Stokes Predictions of Dynamic Stability Derivatives: Evaluation of Steady-State Methods," *Journal of Spacecraft and Rockets*, Vol. 46, No. 6, November-December 2009.
4. Blake, W.B., "Missile Datcom: 1997 Status and Future Plans," AIAA paper 1997-2280.
5. Moore, F.G., *Approximate Methods for Weapon Aerodynamics*, AIAA Progress in Astronautics and Aeronautics, VOL 186, AIAA, Reston, VA, August 2000.
6. Rosema, C., et. al., "Missile DATCOM User's Manual – 2011 Revision," Air Force Research Laboratory Report AFRL-RB-WP-TR-2011-3071, March 2011.
7. Lesieutre, D. J., Love, J. F., and Dillenius, M. F. E., "Recent Applications and Improvements to the Engineering-Level Aerodynamic Prediction Software MISL3," AIAA 2002-0275, Jan. 2002.
8. Moore, F., Moore, L., "The 2009 Version of the Aeroprediction Code: The AP09", API Report No. 3, Jan. 2008.
9. Winchenbach, G.L., "Aerodynamic Testing in a Free-Flight Spark Range," WL-TR-1997-7006, April 1997.
10. Canning, T.N., et. al., "Ballistic Range Technology", AGARD No., 138, August 1970.
11. Owens, D.B. et. al, "Overview of Dynamic Test Techniques for Flight Dynamics Research at NASA LaRC (Invited), AIAA 2006-3146, June 2006.
12. Tomek, D.M., et. al., "The Next Generation of High Speed Dynamic Stability Wind Tunnel Testing," AIAA 2006-3148, June 2006.

13. Hoe., G, Owens, D.B., Denham, C., "Forced Oscillation Wind Tunnel Testing for FASER Flight Research Aircraft," AIAA 2012-4645, June 2012.
14. Billingsley, J.P. and Norman, W.S. "Relationship Between Local and Effective Aerodynamic Pitch-Damping Derivatives as Measured by a Forced-Oscillation Balance for Preliminary Viking Configurations", AEDC-TR-72-25, Arnold Air Force Station, Tennessee, May 1972.
15. Hall, R.M, et. al., "Computational Methods for Stability and Control (COMSAC): The Time Has Come," AIAA 2005-6121, August 2005.
16. Weinacht,P., "Navier-Stokes Predictions of the Individual Components of the Pitch Damping Sum," Journal of Spacecraft and Rockets Vol. 35, No. 5, October 1998.
17. Sahu, J., "Numerical Computations of Dynamic Derivatives of a Finned Projectile Using a Time Accurate CFD Method," AIAA 2007-6581, August 2007.
18. Stalnaker, J., Robinson, M., "Computation of Stability Derivatives Using Unstructured Cartesian Meshes," AIAA 2002-2800, June 2002.
19. Green, L.L., Spence, A.M., "Computational Methods for Dynamic Stability and Control Derivatives," AIAA 2004-0015, January 2004.
20. DeSpirito, J., and Heavey, K.R., "CFD Computation of Magnus Moment and Roll Damping Moment of a Spinning Projectile," AIAA 2004-4713, August 2004.
21. Park, M.A., Green, L.L., "Steady State Compuation of Constant Rotational Rate Dynamic Stability Derivatives," AIAA 2000-4321, June 2000.
22. Murman, S., "A Reduced Frequency Approach for Calculating Dynamic Derivatives," AIAA 2005-0840, January 2005.
23. Etkin, B., Dynamics of Atmospheric Flight, Dover Books on Aeronautical Engineering, September 2005.
24. Chin, S.S., Missile Configuration Design, McGraw Hill Book Co. Inc., 1961.
25. Nielsen, Missile Aerodynamics, McGraw Hill, new York, 1960.
26. Bryson, A.E., "Stability Derivatives for a Slender Missile with Application to a

- Wing-Body-Vertical-Tail Configuration," Journal of the Aeronautical Sciences, Vol. 20. No. 5, May 1953.
27. Weinacht, P., Danberg, J.E., "Prediction of the Pitch-Damping Coefficients Using Sack's Relations," Journal of Spacecraft and Rockets, Vol. 42, No. 5, September 2005.
28. Bolz, R.E. and Nicolaides, J.D., "A Method of Determining Some Aerodynamic Coefficients from Supersonic Free-Flight Tests of a Rolling Missile," Journal of Aeronautical Sciences, 1950.
29. Adams, G.J., Dugan, D.W., "Theoretical Damping in Roll and Rolling Moment Due to Differential Wing Incidence for Slender Cruciform Wings and Wing Body Combinations," NACA-TR-1088, January 1952.
30. Eastman, D.W., "Roll Damping of Cruciform-Tailed Missiles," Journal of Spacecraft and Rockets, Vol. 23, No. 1, January 1986.
31. Barlow, J.B., Rae, W.H., Pope, A., Low Speed Wind Tunnel Testing, Wiley and Sons, Inc., 1999.
32. Bisplinghoff, R.L., Ashley H., Aeroelasticity, Dover Books on Aeronautical Engineering, June 2013.
33. Roskam, J., Airplane Flight Dynamics and Automatic Flight Controls, Roskam Aviation and Engineering Corp, 1979.
34. Murthy, H.S., "Subsonic and Transonic Roll Damping Measurements on Basic Finner," AIAA 1982-4042, January 1982.
35. Regan, F.J., "Roll Damping Moment Measurements for the Basic Finner at Subsonic and Supersonic Speeds," NAVORD Rept 6652, June 1964.
36. Moore, F.G., Swanson, R.C., "Dynamic Derivatives for Missile Configurations to Mach Number Three," Journal of Spacecraft and Rockets, Vol 15 March 1978.
37. Dupuis, A.D., "Aeroballistic Range Tests of the Air Force Finner Reference Projectile," Defence R&D Canada Valcartier, TM 2002-008, May 2002.

38. Uselton and Jenke, "Experimental Pitch and Roll Damping Characteristics at Large Angles of Attack," Journal of Spacecraft and Rockets, vol 14, No. 4., April 1977.
39. Langham, T.F., "Missile Motion Sensitivity to Dynamic Stability Derivatives," AEDC-TR-80-11, September 1980.
40. Ericsson, L.E., "Modification of Aerodynamic Prediction of the Longitudinal Dynamics of Tactical Weapons," LLMSC-D646354, August 1979.
41. Ericsson, L.E., "Missile Dynamics Including High Alpha Manuevers," AIAA 1989-0330, January 1989.
42. Ericsson, L.E., "Wing Body Pitch Damping at Arbitrary Mach Number," AIAA 1980-1801, August 1980.
43. Ericsson, L.E., Reding, J.P., "Effect of Angle of Attack and Mach Number on Slender Wing Aerodynamics," AIAA 1977-0667, June 1977.
44. Chaffin, J.M., "User's Guide for the Bluff Body Aerodynamic Database", MR-TR-1015, July 1979.
45. "Pitching Moment Derivative Due to Rate of Pitch for Projectiles at Supersonic Speeds," ESDU International 910004, May 1991.
46. Weinacht, P., "Prediction of Projectile Performance, Stability, and Free-Flight Motion Using Computational Fluid Dynamics," ARL-TR-3015, July 2003.
47. J.C. Evvard, "Use of Source Distributions for Evaluating Theoretical Aerodynamics of Thin Finite Wings at Supersonic Speeds," NACA report 951, 1950.
48. J.C. Evvard, "A Linearized Solution for Time-Dependent Velocity Potentials Near Three Dimensional Wings at Supersonic Speeds", NASA TN 1699, September 1948.
49. S.M. Harmon and I. Jeffreys, "Theoretical Lift and Damping in Roll of Thin Wings with Arbitrary Sweep and Taper at Supersonic Speeds – Supersonic Leading and Trailing Edges," NACA TN 2114, May 1950.

50. F.S Malvestuto et. al., "Theoretical Lift and Damping in Roll of Thin Wings with Arbitrary Taper and Sweep at Supersonic Speeds – Subsonic Leading Edges and Supersonic Trailing Edges," NACA TN 1860, April 1949.
51. Jones, A.L. and Alkabe, A., "The Damping Due to Roll of Triangular, Trapezoidal, and Related Plan Forms in Supersonic Flow," NACA TN 1548., March 1948.
52. Harmon, S.M., "Stability Derivatives at Supersonic Speeds of Thin Rectangular Wings with Diagonals Ahead of Tip Mach Lines," NACA Report 925, 1948.
53. M. Heiser, "Aerodynamics of a Supersonic Spinning Missile with Dithering Canards", Master's Thesis, Auburn University, May 2002.
54. J. Burkhalter and M. Heiser, "Linear Aerodynamic Analysis of a Supersonic Spinning Missile with Dithering Canards," AIAA paper 2003-2800, June 2002.
55. Brown, C.E., Adams, M.C., "Damping in Pitch and Roll of Triangular Wings at Supersonic Speeds," NACA-TR-892, January 1948.
56. Ribner, H.S., Malvestuto, F.S., "Stability Derivatives of Triangular Wings at Supersonic Speeds," NACA-TR-908, January 1948.
57. Cole, I., Margolis, K., "Lift and Pitching Moment at Supersonic Speeds Due to Constant Vertical Acceleration for Thin Sweptback Tapered Wings with Streamwise Tips: Supersonic Leading and Trailing Edges," NACA TN-3196, July 1954.
58. Martin, J.C, et. al., "Calculation of Lift and Pitching Moments Due to Angle of Attack and Steady Pitching Velocity and Supersonic Speeds for Thin Sweptback Tapered Wings with Streamwise Tips and Supersonic Leading and Trailing Edges," NACA-TN-2699, June 1952.
59. Wilks, B.L., "Aerodynamics of Wrap-Around Fins in Supersonic Flow," Master's Thesis, Auburn University, Decemeber 2005.
60. Moore, F., Moore, L., "New Methods to Predict Non-Linear Roll Damping Moments," Journal of Spacecraft and Rockets, Vol 45, No 5., September 2008.
61. Moore, F., Moore, L., "New Methods to Predict Non-Linear Pitch Damping

- Moments,” AIAA-2008-0215, January 2008.
- 62. Park, S.H., Kwon, J.H., “Navier Stokes Computations of Stability Derivatives for Symmetric Projectiles,” AIAA 2004-0014, January 2004.
 - 63. Despirito, J., Silton, S.I., Weinacht, P., “Navier Stokes Predictions of Dynamic Stability Derivatives: Evaluation of Steady State Methods,” ARL-TR-4605, September 2008.
 - 64. ”Experimental Roll Damping, Magnus, and Static Stability Characteristics of Two Slender Missile Configurations at High Angles of Attack (0 to 90 Deg), AEDC TR-76-58, July 1976.
 - 65. Mikhail, A.G., “Roll Damping for Finned Projectiles Including: Wraparound, Offset, and Arbitrary Number of Fins,” AIAA paper 1993-3460, August 1993.
 - 66. Auman, L.M., and Kirby-Brown, K., “MissileLab User’s Guide,” Technical Report AMR-SS-09-04, Redstone Arsenal, AL, February 2009.